3-31-2018

Pore-Scale Analysis of Interfacial Instabilities and Impact of Heterogeneity on Relative Permeability by Lattice Boltzmann Method

Zhipeng Zhu
Louisiana State University and Agricultural and Mechanical College, zzhu12@lsu.edu

PORE-SCALE ANALYSIS OF INTERFACIAL INSTABILITIES AND IMPACT OF HETEROGENEITY ON RELATIVE PERMEABILITY BY LATTICE BOLTZMANN METHOD

A Thesis

Submitted to the Graduate Faculty of the
Louisiana State University and
Agricultural and Mechanical College
in partial fulfillment of the
requirements for the degree of
Master of Science

in

The Craft & Hawkins Department of Petroleum Engineering

by
Zhipeng Zhu
B.S.P.E., Missouri University of Science and Technology, 2015
May 2018

ACKNOWLEDGEMENTS

I'm very grateful for the help, guidance and support I received from, my advisor, Dr. Tyagi and my committee members: Dr. Hughes and Dr. Thompson. Dr. Tyagi helped me with his knowledge on fluid flow and numerical methods as well as encouraged me with his experience when he was a graduate student.

I appreciate TA funding from Craft & Hawkins Department of Petroleum Engineering.

I appreciate Dr. Le Yan and Dr. Feng Chen for their support and resources of HPC.

At last, I'm thankful for the support and encouragement from my parents. I wouldn't have made it this far if they had not been always by my side.

TABLE OF CONTENTS

LIST OF TABLES

LIST OF FIGURES

ABSTRACT

Interfacial instabilities occur often during immiscible fluid flow through porous media and their understanding is essential for waterflooding operations or other oil recovery processes. Although many studies including experimental and numerical have been done to reproduce and analyze the interfacial instabilities in porous median, there is still significant knowledge gap in fundamental understanding of these flow instabilities at the pore-scale. In order to better understand the interfacial instabilities phenomenon, the pore-scale simulations are performed. In this study, Lattice Boltzmann Method is used to simulate two different types of interfacial instabilities: viscous fingering and capillary fingering in irregular sphere packs by changing the viscosity ratio of the displacing and displaced fluid to achieve different force balances. A distinct feature of viscous fingering at the pore scale is that the wetting phase mostly flows through the pore space such that a sharp interface between immiscible fluids in pore space is observed while it sporadically moves along the grain surface. In contrast during the capillary fingering instabilities, the wetting phase moves mainly along the grain surface. Further, the fluid flow paths during different instabilities can be significantly different even in the same porous medium. Also, the effective relative permeability is calculated while accounting for heterogeneity in the porous media. Based on the simulation results it was concluded that heterogeneity in porous media will in general lower relative permeability of wetting phase during the imbibition process but may not significantly influence the non-wetting phase relative permeability.

CHAPTER 1. INTRODUCTION

Waterflooding is the most widely used oil recovery method all around the world, the efficiency of water flooding depends on many factors. Among all the factors, the behavior of oil-water interface and relative permeability functions are two of the most important factors. Since Hill(1952) observed that when one fluid is displacing the other fluid, the interface is finger-shaped. Many researches have been done experimentally and numerically to explore interface instability and its mechanism. the mechanism of the viscous fingering in oil-water system is firstly well explained by Saffman–Taylor (1958) who did the experiment to reproduce viscous fingering in a Hele-Shaw cell. Later on, the instability caused by capillary force was observed and illustrated. However, not many of the studies have been done in pore-scale. This study will focus on qualitatively analysis of two types of interface instabilities in pore-scale: viscous fingering and capillary fingering and quantitatively determine how heterogeneity alters the effective relative permeability. Better understanding of the interface instability and relative permeability are very important for reservoir engineers to obtain more accurate simulation results.

In this study, Lattice Boltzmann method (LBM) Shan-Chen multiphase model was used to simulate oil-water multiphase flow in pore-scale. The periodic uniform sphere packs were used as the porous media. By changing the viscosity ratio of the displacing fluid over the displaced fluid, the interface instability caused by viscous force and capillary force were simulated. The result shows that in the same porous media, the interface shape and the flow path of capillary force dominated flow is different from the viscous force dominated flow. The main feature of the viscous fingering is the sharp interface appears in the pore space however, the sharp interface of capillary fingering appears along the grain surface. As far as investigating how

heterogeneity affects relative permeability, the heterogeneity was created by placing uniform sphere pack and other two sphere packs which are random sphere packs with different sphere radius perturbation in serial. By fixing the water saturation and running the simulation to steady state, the relative permeability of each sphere pack and the whole system at this one water saturation can be determined. Then the relative permeability curves were generated by this method. The comparison of relative permeability curves states that the wetting phase relative permeability was lowered by the heterogeneity especially in high wetting phase saturation. But the non-wetting phase relative permeability were not greatly altered by heterogeneity.

CHAPTER 2. LITERATURE REVIEW

An overview of various simulation techniques that have attempted to address the issue of interfacial instabilities at the pore scale is presented here. By no means, this literature review is exhaustive and the readers are directed to Blunt (2017).

2.1. Numerical Method Used in Pore-Scale Modeling

There are many numerical methods for simulating multiphase fluid flow in porous medium in pore-scale. The models developed to solve multiphase fluid flow through porous media can be classified into rule-based and first-principle-based models. Rule-based models were developed to capture the physics of multiphase flow in porous media in idealized porous media models. The rule-based models include diffusion-limited aggregation models, Percolation models and pore-network models.

2.1.1. Pore-Network Model

Pore network model is one of the most widely used for pore scale modeling for last decades. In pore network model, porous media were idealized to the structure that has pore throats and wide pores. Fatt (1956) is the first one who used pore network model to simulate pore–scale multiphase flow and determined relative permeability and capillary pressure. After that, more and more researchers started using pore network model for pore scale modeling and more physics have been incorporated by pore network models. The recent research done by Hilpert (2001) have adapted mathematical morphology analysis of actual porous media to the pore network model. It was done by matching the morphological pore-size distribution and the genus of the network with those of the porous medium. Marcke (2007) built the pore network

model by extracting the network of sandstone pore space image. The algorithm computes the location and sizes of pores and throats and then create a pore network model for actual experiment image of the 3D sandstone image. There are several advantages of using pore network modeling: sharp interfaces, high resolution, low computational cost. The model has been developed to simulate the real rock by adding random pore networks, pores with angular cross-sections, wettability. However, the limitation of pore network model is that the pore structure is still based on simplified and idealized network and the interaction between fluid and complex geometry can't be simulated.

2.1.2. Coarse-Grain Method

The first-principle-based methods solve the governing equations of the fluid flow which is the Naiver–Stokes equation. The governing equations can either be solved by fine-scale methods or coarse-grain methods. The coarse-grain method solves the governing equation with boundary conditions by discretize the governing equation using finite difference, finite volume or finite element methods. The limitation of coarse-grain methods is the difficulty of implementing the boundary conditions of two-phase flow for complex rock geometry. In order to overcome the difficulty, Harlow (1965) firstly developed the front-capturing model in which the boundary is partially confined and partially free, and the model used a set of marker particles which move with the fluid which is called marker and cell method.

2.1.3. Volume of Fluid (VOF) Method

Hirt (1981) developed the finite difference numerical model by using Volume of Fluid (VOF) method to tract free fluid surface in complex geometry. Fast Marching Methods and Level Set methods were introduced by Sethian (1996), they can be used to track complex 3D

fluid fronts in pore scale. Tryggvason (1991) simulated multiphase fluid flows with sharp interface by using a front-tracking method in which the flow field is discretized by a finite difference approximation on a stationary grid, and the interface is explicitly represented by a separate, unstructured grid. However, it's still challenging to simulate multiphase flow in complex porous media by traditional CFD method.

2.1.4. Molecular Gas Dynamics Method

Molecular Gas Dynamics Method by Bird (1994) provided a different way to simulate fluid flow which takes the movements and collisions of all the molecules in the fluid into account with intermolecular interactions and gives realistic equations of state of fluid. However, because the large amount number of molecules and interactions needed to represent macroscopic fluid flow, this method can't be used for modeling fluid flow in pore scale.

2.1.5. Pore Morphology(PM) Model

Another pore-scale simulation model is the pore morphology model. The PM models find the relationship between the macroscopic properties of a porous medium such as: capillary pressure, flied saturation and the representation of the porous medium by using mathematical morphological analysis. In the work of Hazlett (1995), he constructed the algorithm for capillary dominated displacement and the displacement can be computed based on the capillary pressure. Later on, Hilpert and Miller (2003) used pore morphology model to determine the fluid distribution in a quasi-static drainage in water-wet porous medium but the pore space was discretized a set of voxels on a cubic lattice. Furthermore, Volker (2015) modified the pore morphology model by treating partially wetting porous media directly in the simulation reproduced capillary pressure-saturation curves. The advantage of Pore Morphology method is

that it doesn't require as much as computational time and memory compared to other multiphase flow models.

2.1.6. Lattice Boltzmann Method

Lattice Boltzmann method is another alternative CFD method for simulating fluid flow in pore scale. It emerged in 1980s and it started becoming a great method for simulating mesoscopic fluid dynamics. LBM has been widely used in different fields of fluid flow problems such as: biologic, cell-fuel and etc. In LBM, discrete Boltzmann equation is solved to simulate the flow of a Newtonian fluid with collision models, instead of solving the Naiver–Stokes equations.

2.2. Pore-Scale Modeling by Using LBM

As far as using LBM for simulation of complex fluid flow in porous media, Succi et al. (1989) validated the lattice Boltzmann modeling for fluid simulation in complex 3D porous media geometries. More and more researches have been using lattice Boltzmann modeling to solve fluid of single phase or multiphase problems in porous media.

2.2.1. Single Phase LBM Pore-Scale Modeling

After Succi's et al. (1989) work, more and more researches started adapting LBM for simulation of fluid flow in pore-scale, Rothman (1995) simulated single phase flow in Fountainbleau sandstone. LB models have been used to investigate single-phase flow in different porous media including, sphere packings done by Maier et al. (1998) and Chukwudozie (2011) used lattice Boltzmann method modeled the fluid flow in sphere packs and calculated the permeability, tortuosity and other flow parameters for single phase flow, cemented media, and

media with random obstacles. Later on Jin et al. (2004) used the physics based reconstruction approach to create virtual samples of consolidated and unconsolidated reservoir rocks simulated fluid flow in the virtual rock sample and calculated the absolute permeability.

2.2.2. Multiphase LBM Pore-Scale Modeling

A few LBM models have been developed for modelling multiphase fluid flow systems in LBM. The earliest one is the chromodynamics model developed by Gunstensen (1991). Later on, the pseudo-potential model which is known as Shan-Chen model was developed Shan and Chen (1993). Multiphase flows in porous media are usually simulated numerically by using macro-scale simulations, where continuity equation is solved with mass and momentum balance and Darcy's law. However, since this method is using macro-scale simulation, therefore, it has difficulties in solving problem in complex pore geometry with heterogeneity. In addition, Traditional Computational Fluid Dynamics (CFD) methods simulate multiphase flows by solving macroscopic Naiver-Stokes equations, which is not an optimal choice for simulating flows in porous media. With the development of high performance computing, Lattice Boltzmann method (LBM) has been used to solve fluid flow problems in engineering. LBM is unlike traditional CFD methods, it's a pseudo-molecular method that tracks the evolutions of the particle distribution and the macroscopic variables are computed based on moments of particle distribution. There are many studies have been done by using LBM for fluid flow problems.

Recently, LBM based multiphase pore-scale simulation have utilized Shan-Chen model in many studies. Chen (2011) used Shan-Chen model to simulate the viscous fingering in 2D tube and CO2 and water flow in 3D image of sandstone. Genty (2013) worked in simulation of multiphase flow: Liquid and gas in porous media(soil) validated the Shan-Chen model with

analytical solution and obtained 3D map of liquid and gas distribution in soil. Shan-Chen model has also been used to simulate multiphase flow and reactive transport in pore-scale, Chen (2013). Later, Landry (2014) focus on pore-scale fracture-matrix fluid transportation and the process of water with surfactant displacing oil in oil-wet fractured porous media was reproduced and compared with experiment result. In simulating multiphase fluid flow via LBM, color gradient model has been used in order to investigate the relative permeability in pore scale and the influence of viscosity ratio in water flooding. Latva-Kokko (2005) implemented the phase contact angle in color gradient model. Later on, many researches on multiphase flow in porous media were done by color gradient model. The advantage of color gradient model is that the interfacial tension can be adjust for different cases. Multiphase Volume of Fluid (VOF) method can also be used for pore scale multiphase fluid simulations as well. However, the difficulty of using this method is to eliminate the smearing of the free surface Boek et al. (2010). Swift (1995) introduced Free energy model for multiphase fluid system. In this study, Shan-Chen model is used to simulate fluids with different viscosities and densities for interface tracking and contact angle adjustment between fluid and rock geometry.

2.2.3. Advantages and Disadvantages of LBM in Pore-Scale Modeling

The advantages of lattice Boltzmann method (LBM) are: dealing with complex boundaries, incorporating microscopic interactions, and parallelization of the algorithm. However, the disadvantage is it has limitations related to finite resolution and relies on the simplified collision and propagation scheme of fluid distributions.

2.3. Interfacial Instabilities

In this section, viscous instabilities and capillary instabilities in the porous media are discussed.

2.3.1. Instability Phenomenon and Related Experiment

Water flooding is the most widely used oil recovery method around the world in last century, it provides us the way to maintain the reservoir pressure and at the same time displace the oil from the reservoir. The injected water in the oil reservoir forms an advancing front whose saturation at the front varies greatly due to the instability at oil water interface, this is usually called "Fingering". The instability of interface in oil recovery process is usually caused by viscous contrast of injected water and oil. Fingering will lead to poor water sweep efficiency in the reservoir, lower relative permeability and early water breakthrough. The immiscible displacement process in porous media is controlled by capillary and viscous force. Therefore, the fingering phenomenon can be divided into viscous fingering, capillary fingering and the transition zone in between. Capillary Number $Ca = \frac{v\rho V}{\gamma}$ where v is the average viscosity of fluid, ρ is average density of fluids, V is the flow velocity and γ is surface tension, and viscosity Ratio $\mathrm{M} = \frac{\mu_{\mathrm{displacing}}}{\mu_{\mathrm{displaced}}}$ are used to quantify the transition between viscous fingering and capillary fingering. However, in some situations, the fingering can be caused by the heterogeneity in porous media Tchelepi (1994). There are many works have been done to investigate the phenomenon and mechanism of interfacial instabilities. The structure of viscous fingering caused by mobility ratio difference was observed by Hill(1952), he observed that when one fluid is displacing the other fluid, the interface is finger-shaped, the mechanism of the viscous fingering in oil-water system is well explained by Saffman–Taylor (1958) who did the experiment to reproduce viscous fingering in a Hele-Shaw cell which is shown in below in Figure 2.1. As far as experimental studies on viscous fingering, Chuoke et al. (1959) simulated macroscopic interface instabilities of the one fluid displacing another immiscible fluid in uniform porous medium.

Homsy (1985) investigated how surface tension contributes to the instability. Homsy (1991) investigated the impact of anisotropic dispersion on nonlinear viscous fingering in miscible displacement process and at the same time stated that the Hele-Shaw cell can't be used to investigate interfacial instability in porous media because the model neglected propagation of the menisci through the pore space. Garik (1990) did the experiment of viscous fingering in anisotropic formation. Later on McCloud and Maher (1995) reviewed Saffman–Taylor's experiment and explained the theory of dynamics of driven interface by adding perturbations to the Saffman–Taylor flow.

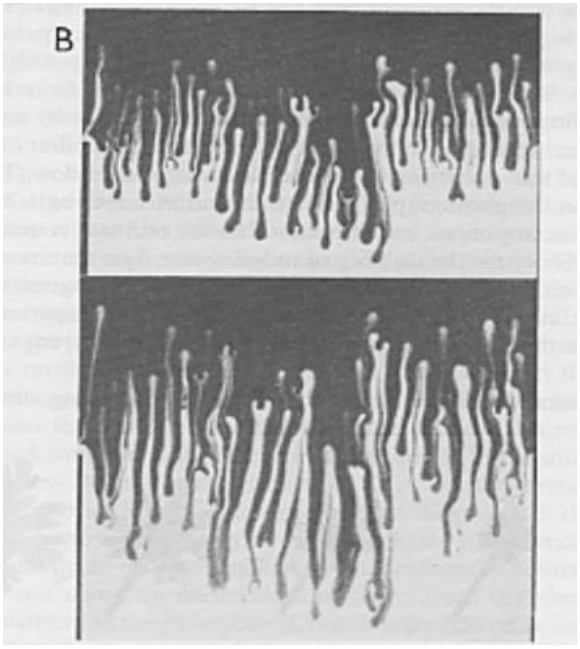

Figure 2.1. Fingering in a Hele-Shaw model by Saffman–Taylor (1958) in gravity drive miscible displacement

For displacement process in very low flow velocity, the aspect ratio of pore structure can be large, and it will cause the heterogeneity of capillary pressure along the interface. The interfacial instability caused by capillary force. Capillary fingering phenomenon have been studied by many researchers. Wilkinson (1983) introduced Invasion percolation with

trapping(IPT) model to investigate the capillary fingering and later on many studies were done by using IPT model. Lenormand (1989) did experiment and showed capillary fingering in 2-D porous medium model and addressed on theoretical model of capillary fingering by using fractal dimension. When it comes to finding the cross-over zone, in the work of Lenormand (1988), a phase diagram was firstly developed to describe the transition between stable displacement, viscous fingering and capillary fingering. Later on, more researches focused on it have been done both experimentally and numerically.

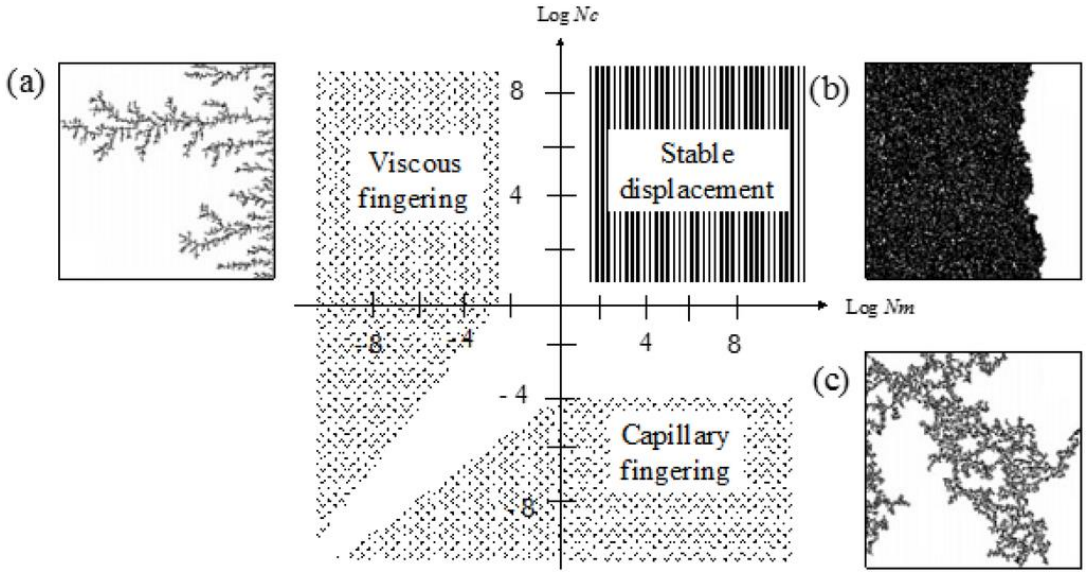

Figure 2.2. Phase diagram developed by Lenormand et al. (1988) shows the threshold value of the fingerings

As far as the interface instability in pore-scale, Nakken (2012) used micromodels reproduced the fluid displacement in multiphase system. He visualized and analyzed the fluid flow physics including viscous fingering, capillary fingering and contact angles. Later on, Ran (2016) investigated the effect of pore size disorder on fluid displacement coupled with capillarity, viscosity and wettability.

2.3.2. Numerical Simulations of Interfacial Instability

When it comes to numerical simulation of viscous fingering, many researchers have been using different numerical model to analyze the mechanism of fingerings and the pattern of the instabilities. Peaceman and Rachford (1962) developed a system of partial differential equations which take into account of gravity, diffusion, and fluid viscosities and densities and the spatial distribution of permeability for miscible fluids displacement in porous media and the simulation result quantitatively shows agreement with experiment data. The later studies did by Yortsos and Zeybek (1988) examined the effect of dispersion on the instability phenomenon. Numerical simulation is another important tool to investigate viscous fingering in pore scale.

Manickam and Homsy (1995) used linear stability analysis and direct numerical simulations to simulate the fingering in vertical miscible fluid displacement in porous media driven by both viscosity and density differences. Clemens et al. (2013) developed a CFD model which uses images of the porous medium obtained by a Scanning Electron Microscope (SEM). The governing equation: Naiver-Stokes equation combined with mass and momentum conservation was solved subsequently. The model successfully determined the phase saturation in the pore space and shows the viscous fingering in water flooding oil recovery process. Regaieg (2017) used pore network model investigated the flow pattern of water displacing heavy oil in homogeneous porous medium. Another method for simulating viscous effect is LBM. Researchers have been using it in simulation of viscous fingering phenomenon in Hele-Shaw cell and in porous media. Dong (2011) simulated viscous fingering in immiscible flooding process by using LBM, the result of Hele-Shaw shows good agreement with experiment result qualitatively. The simulation of immiscible displacement process in simplified porous medium shown in

Figure 2.5 with different dimensionless numbers, capillary number, Bond number has been done in his work as well in order to show the fluid flow pattern in different condition.

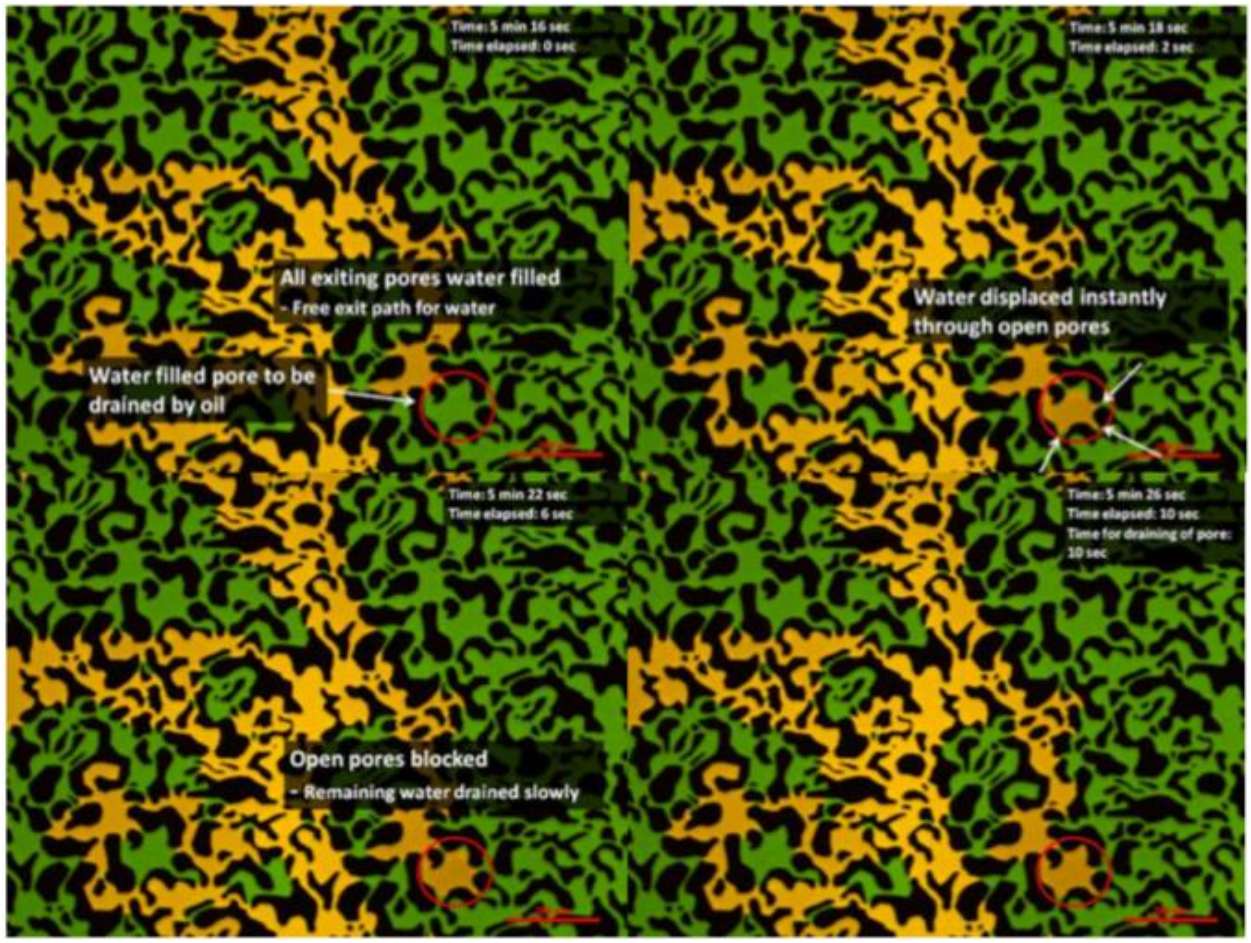

Figure 2.3. Nakken(2012) used micromodels to simulate multiphase flow in porous media and visualized the displacement process of capillary fingering

Liu (2013) Used high-density ratio model reproduced the fluid flow in porous media and investigated the influence of capillary number, viscous ratio, contact angle and bond number to the flow regime. However, the transition of instability mechanism between viscous fingering and capillary fingering is slightly different result from Lenormand et al. (1988) due to the difference of pore structures. The other instability mechanism is caused by capillary force. When it comes to water flooding, due to most of the oil reservoir world the world consists of water wet reservoir rock, the process can be seen as water imbibition. The displacing fluid which is water will get in

the smallest pore throat where the capillary pressure is the highest. In porous medium, the mean curvatures of the pore space vary greatly which will lead to large change of the magnitude of capillary pressure. In this situation, when the fluid is injected with low flow rate which will drastically decrease the viscous force and the fluid becomes capillary dominant, therefore the displacing mechanism is controlled by the pore size and capillary force.

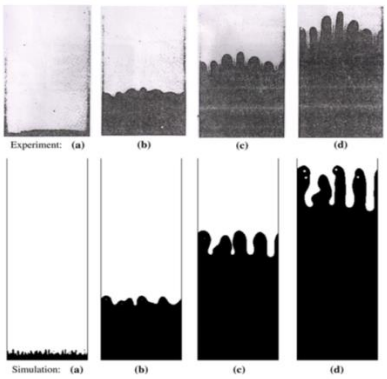

Figure 2.4. The numerical simulation result of viscous fingering in Hele-Shaw done by Dong (2011) by using LBM

Investigator has put great effort on simulate and observe capillary fingering in experiment and numerical simulation. Riaz (2004) used linear stability analysis to investigate the length and

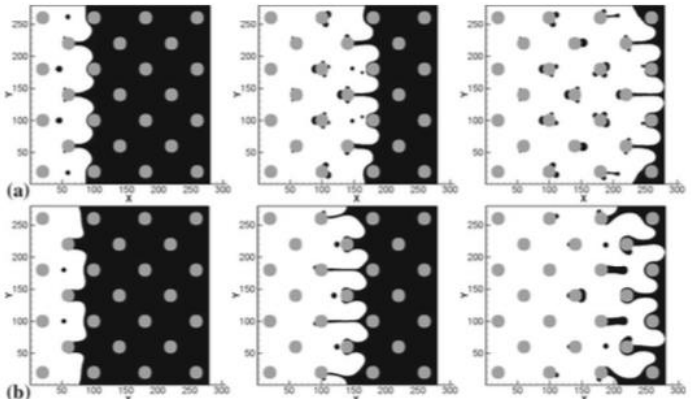

Figure 2.5. By Dong (2011), altered the viscosity ratio of displacing fluid and displaced fluid: a) M=1 b) M=2. The shape of viscous fingers for larger M is flatter than case with small M.

size of fingering. In the work of Yiotis et al. (2007) the effects of capillary force in pore scale cause by wettability between interface of solid geometry and fluid was investigated.

Mukherjee (2010) adapt Shan-Chen model to simulate air and water flow in fuel-cells, he showed that as the increase of capillary pressure during the displacement process, the flow regime transit from capillary fingering to stable displacement. The finger shaped interface disappears with time. However, there are not many works that have been done to investigate capillary fingering in immiscible water-oil system in pore scale numerically.

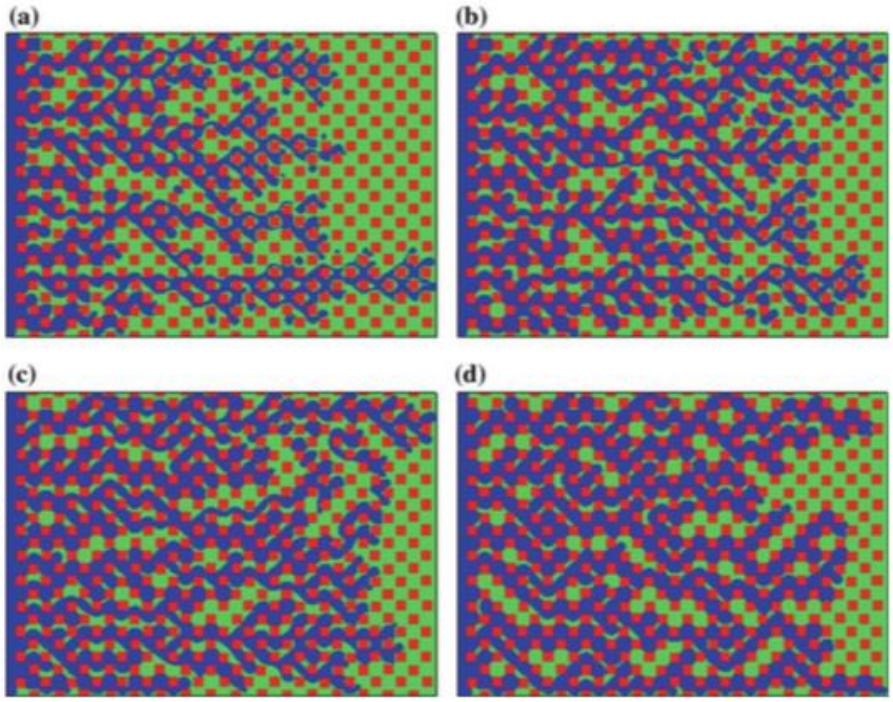

Figure 2.6. In Liu's (2013) research, the interface pattern with various viscosity ratios a M=1/100, b M=1/40, c M=1/20, d M=1/5

2.4. Relative Permeability and Its Determination by Numerical Methods

Permeability is rock property which is used to describe the ability of a porous media to allow fluid to flow through it. The magnitude of permeability is related to the porosity of the

porous media and the shape of pores in the porous media. When there is only one phase of the fluid flowing through the porous media, the ability of the porous media to conduct flow fluid is called “absolute” permeability. However, when there are two or more immiscible fluid flowing through the porous media, “relative” permeability is used to describe the ability of the porous media transmits a particular fluid through it.

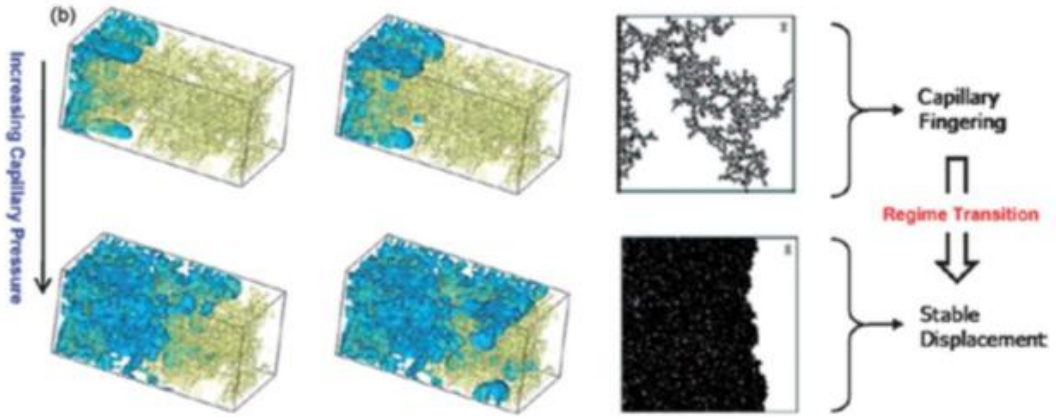

Figure 2.7. Mukherjee (2010) used LBM Shan-Chen model to simulate displacement process in porous media(fuel-cell)

Nowadays, reservoir simulation is becoming more and more powerful with the development of the computer. It has been used to making production plan and design oil recovery patterns for decades. The significance of determining relative permeability accurately for water and oil system is that it can help predict flow pattern in water flooding and optimize the oil recovery process. Not like absolute permeability which is purely a property of rock, Relative permeability is related not only to the rock, but it’s also affected by the fluid properties, the interaction between fluid and fluid and interaction between fluid and rock. In most circumstance, the relative permeability is measured by using experimental method. The most widely used

methods are unsteady-state method, steady-state method and centrifuge method. The disadvantages of experimental approaches are: they are very time consuming and it's difficult to perform in the actual reservoir condition. Therefore, researchers started using numerical methods for the determination of relative permeability. Pore Network models were widely used to determine the relative permeability of the rock. Roth (1998) generated pore-network by using the serial sectioning technique and then simulated the fluid flow in soil and calculated the relative permeability. Later on, Blunt (2000) simulated multiphase flow in porous medium, they reproduced primary drainage process and determined water flooding relative permeability curves for Berea sandstone using pore network model. Blunt et al. (2002) used pore network model to reproduce capillary pressure curves and relative permeability curves for a given rock. In the work presented by Jin et al. (2004), the pore network model was constructed from 3D image of porous medium and the imbibition relative permeability curves were determined. Piri and Blunt (2005) developed the pore network model which adapted many features of multiphase fluid flow in pore-scale which includes hysteresis, wettability alteration and etc. Based on this model the relative permeability curves and capillary pressure for different displacement sequence were determined and the simulation results have a good agreement with experiment results for water-oil system in porous medium. Although Pore network models have been using for decades for determination of relative permeability and it has many advantages for simulating multiphase fluid flow in porous medium - it gives sharp interfaces, adapted a great amount of pore scale fluid physics and computationally cheap yet many limitations still exist.

The other method which is used more and more often in the last decade for determination of relative permeability curves is Lattice Boltzmann Modeling. Boek (2010) used Lattice Boltzmann simulation to determine the relative permeability curves for realistic rock sample by

doing 2D simulation and then using an effective drag force to represent the third dimension. Akshay and Tayfun's (2010) estimated relative permeability for matrix-fracture interaction using LBM simulations. The 2D LBM model was built to investigate the relative permeability of fractures. Keehm and Mukerji (2010) obtained the relative permeability curves in X-ray microtomograph 3D models of different samples of Fontainbleau sandstone. Later on, Ramstad et al. (2012) built the model with X-ray micro-tomography of pore-space images and simulated two phase flows by Lattice Boltzmann method. The relative permeability curves were determined in steady-state and unsteady-state and the result shows good agreement with experiment results.

CHAPTER 3. PROBLEM STATEMENT AND RESEARCH OBJECTIVES

Water flooding is the most widely used oil recovery method around the world. During the fluid-fluid displacement processes, many factors can influence the areal sweep efficiency of water flooding operations. Fundamental understanding of the multiphase fluid flow behavior in porous media is essential since it has a great impact on the oil recovery factory in flooding process. Due to the difference in the viscosity of displacing/displaced fluid and the corresponding capillary force, the fluid-fluid interface can become unstable thus leading to poor sweep efficiencies at the reservoir scale. In this study, the interfacial instabilities in multiphase system in pore-scale will be simulated by using LBM and *instabilities caused by viscous force and capillary force will be analyzed* qualitatively through detailed visualizations.

From reservoir perspective, the heterogeneity of rock due to different grain size or packing of the grain will change the relative permeability in different areas of the reservoir that in turn could lead to poor macroscopic sweep efficiency at the reservoir scale. Typically, reservoir simulations are carried out to select/design a water flooding pattern. For heterogeneous property reservoir simulation, permeability and relative permeability curves are the key properties that could control the spatial saturation variability for each fluid phase. Therefore, our objective in this study is also to investigate *how heterogeneity can influence the relative permeability curves* in order to provide accurate prediction of flow pattern and oil recovery factor for oil reservoir simulation.

CHAPTER 4. OVERVIEW OF LBM AND SHAN-CHEN MULTIPHASE MODEL

4.1. Lattice Boltzmann Method

Boltzmann's theory stated that gas system is a system consists of a number of interaction particles that can be described by using classical mechanics and statistical treatment. Therefore, any fluid system can be described by using distribution function $f^{(N)}(x^N, p^N, t)$, where N is the number of particles, x is the position vector and p is the momentum vector, and t is the time. Changes in distribution function with time are given by the Liouville equation. However, this level of description is not possible for real gas, where there are 10^{23} particles that involved in a mole of gas. However, we are usually only interested in lower order (1,2) functions. Therefore, the Boltzmann equation can be derived from the first order distribution function:

$$v \cdot \nabla_x f^{(1)} + F \cdot \nabla_x f^{(1)} + \frac{\partial f^{(1)}}{\partial t} = \Gamma^{(+)} - \Gamma^{(-)} \tag{4.10}$$

The lattice Boltzmann model is built from the simplified Boltzmann equation in which the particles positions are confined to the node of lattice and the variation of momenta are reduced to the specific amount of directions n. (n can be 8 for 2D system and 15 or 19 for 3D system). This LBM classification scheme was proposed by Qian et al. (1992) for 2D system with 8 directions of velocity direction (D2Q9) which is shown in figure below. The velocity magnitude of $e_1$through e_4 is 1 lattice unit per time step (1 lu ts-1). The velocity magnitude of e_5 through e_8 is $\sqrt{2}$ lattice unit per time step ($\sqrt{2}$ lu ts-1) Based in the D2Q9 model, the distribution function will be discrete instead of continuous. Then the frequencies of occurrence can be used to express the macroscopic density:

$$\rho = \sum_{i=0}^{8} f_i \tag{4.11}$$

Then the macroscopic velocity u can be expressed as an average of microscopic velocities e_i weighted by the directional densities:

$$u = \frac{1}{\rho}\sum_{i=0}^{8} f_i e_i \tag{4.12}$$

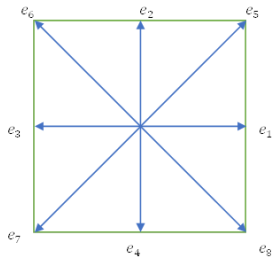

Figure 4.1. The velocity directions of D2Q9 Lattice Boltzmann model. 2D model with 8 directions of velocity

After that, The BGK (Bhatnagar-Gross-Krook) Approximation for collision and streaming can be applied. The BGK approximation is:

$$f_i(x + e_i\Delta t, t + \Delta t) = f_i(x,t) - \frac{1}{\tau}[(f_i(x,t) - f_i^{eq}(x,t)] \tag{4.13}$$

in which τ is the relaxation term which is related to the kinematic viscosity of the fluid, $f_i(x + e_i\Delta t, t + \Delta t) = f_i(x,t)$ is the streaming part and $\frac{1}{\tau}[(f_i(x,t) - f_i^{eq}(x,t)]$ is the collision part. $f_i^{eq}(x,t)$ is the D2Q9 equilibrium distribution function which is defined as

$$f_i^{eq}(x,t) = \omega_i \rho(x)\left[1 + 3\frac{e_i \cdot u}{c^2} + \frac{9(e_i \cdot u)^2}{2c^4} - \frac{3u^2}{2c^2}\right] \tag{4.14}$$

in which ω_i are weights (4/9 for rest particles (a=0), 1/9 for a=1,2,3,4, and 1/36 for i= 5,6,7,8) and *c* is the basic speed on lattice (1 lu ts-1). In LBM, there are other models such as D3Q15 or D3Q19 models and they will have different equilibrium distribution functions for themselves.

The D3Q19 model will be used in our work, shown below in Figure 4.2. The 3-D model contains 18 velocity vectors in each lattice node and 1 rest distribution which is the center of the lattice node.

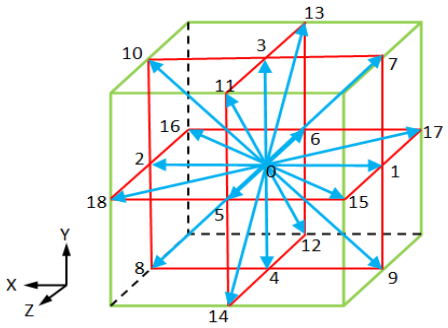

Figure 4.2. The velocity directions of D3Q19 LB model, D3 means 3D model and Q19 means the microscopic momentum has been discretized to 19 directions.

The equilibrium distribution function for D3Q19 model is defined as

$$f_i^{eq}(x,t) = w_i \rho(x) \left[1 + 3e_i \cdot u + \frac{3}{2}(3(e_i \cdot u)^2 - u^2)\right] \tag{4.15}$$

in which w_i is a weight factor related to velocity vector i

$$w_i = \begin{cases} \frac{1}{3}, & for\ i = 0 \\ \frac{1}{18} & for\ i = 1, \dots, 6 \\ \frac{1}{36} & for\ i = 7, \dots, 18 \end{cases} \tag{4.16}$$

The BGK (Bhatnagar-Gross-Krook) Approximation for collision and streaming can be applied. The BGK approximation is:

$$f_i(x + e_i\Delta t, t + \Delta t) = f_i(x,t) - \frac{1}{\tau}[(f_i(x,t) - f_i^{eq}(x,t)] \quad (4.17)$$

where τ is the relaxation time to equilibrium which is related to kinematic viscosity of the fluid as:

$$\tau = \frac{6v+1}{2} \quad (4.18)$$

the local fluid pressure is calculated based on ideal gas law, $p = c_s^2\rho$, where c_s is the speed of sound in lattice unit and $c_s = \frac{1}{\sqrt{3}}$.

As far as unit conversion from physical unit to lattice unit, it uses some dimensionless parameter as the intermediate bridge such as Reynold's number. Because if two system has the same Reynold's number, then the two systems represent the same physics. The time step Δt for lattice Boltzmann model will be set first based on the Δx in the model. In order to ensure the numerical stability, the time step Δt must be set to be 100 times less than Δx.

4.2. Introduction to Shan-Chen Model

Shan-Chen model was proposal by Shan and Chen in 1993, they proposed single component multiphase model(SCMP) and multi-component multiphase model(MCMP). Here the MCMP is what will be used, and it will be introduced here briefly.

Shan-Chen model has been widely used for multiphase flow simulation for oil and water system and in Shan-Chen MCMP model, the interaction between particles is a repulsive force which leads to the phase separation and interface maintenance Edo S. Boek. et. al. (2010). In

Shan-Chen model, it introduces one distribution function to each fluid and the distribution function is shown below:

$$f_i^{\sigma}(x + e_i\Delta t, t + \Delta t) = f_i^{\sigma}(x,t) - \frac{1}{\tau_\sigma}(f_i^{\sigma}(x,t) - f_i^{\sigma,eq}(x,t))) \tag{4.19}$$

in which $f_i^{\sigma}(x,t)$ is the σth component density distribution function in the ith velocity direction and $\tau_\sigma$is a relaxation time in the BGK model which has the relationship between the kinetic viscosity as:

$$v_\sigma = c_s^2(\tau_\sigma - 0.5\Delta t) \tag{4.20}$$

and $f_i^{\sigma,eq}(x,t)$ is the equilibrium distribution function which can be defined as:

$$f_i^{\sigma,eq}(x,t) = \omega_i\rho_\sigma\left[1 + \frac{e_i\cdot u_\sigma^{eq}}{c_s^2} + \frac{(e_i\cdot u_\sigma^{eq})^2}{2c_s^4} - \frac{u_\sigma^{eq2}}{2c_s^2}\right] \tag{4.21}$$

In equation 4.19 and 4.20 the e_i is the discrete velocities and c_s is the square of the speed of sounds which is $c_s = \frac{c}{\sqrt{3}}$ and $c = \frac{\Delta x}{\Delta t}$ in lattice unit. And the density of σth component's density is:

$$\rho_\sigma = \sum_i f_i^{\sigma} \tag{4.22}$$

Then the macroscopic velocity u_σ^{eq} for each phase can be defined by:

$$u_\sigma^{eq} = u' + \frac{\tau_\sigma F_\sigma}{\rho_\sigma} \tag{4.23}$$

in which u' is a velocity common to the various components and defined as:

$$u' = \frac{\sum_\sigma (\sum_i \frac{f_i^\sigma e_i}{\tau_\sigma})}{\sum_\sigma \frac{\rho_\sigma}{\tau_\sigma}} \tag{4.24}$$

and F_σ is the force that acts on the σth component which is the sum of fluid-fluid cohesion $F_{c,\sigma}$ and fluid-solid adhesion $F_{ads,\sigma}$.

In multiphase model, each node is filled with more than one fluid. Therefore, the overall fluid density over the computational domain can be calculated as

$$\rho = \sum_\sigma \rho_\sigma \tag{4.25}$$

The pressure calculation in MCMP Shan-Chen model is different from single phase lattice Boltzmann model, the pressure is directly related to the cohesion force.

The cohesion force that acts on the σth component is defined Shan and Doolen (1995)

$$F_{c,\sigma} = -G\psi_\sigma(x,t)\sum_i \psi_{\bar{\sigma}}(x + e_i\,\Delta t, t)e_i \tag{4.26}$$

where ψ_σ is the effective mass (Shan and Doolen 1995) which is a function of local density. Here we use $\psi_\sigma = \rho_\sigma$ Shan and Doolen (1995). Based on the velocity in D3Q19 model, by applying Taylor's series expansion to $\psi_{\bar{\sigma}}(x + e_i\Delta t, t)$ and then compare with momentum flux tensor with the diffuse interface method. The pressure can be obtained as:

$$p = c_s^2\rho + 12c^2 G\rho_1\rho_2 \tag{4.27}$$

However, in Shan-Chen model, the interfacial tension can't be changed, which will lead to the fluid to be compressible. In present, this problem can't be fix by changing parameters for the Shan-Chen model.

4.3. Unit Conversion Between Physics Unit and LB Unit

The fluid property and flow parameters in the LBM are all in LB unit, which are different from physics unit in the realistic case. The bridge needed to connect the physics unit and LB unit is usually dimensionless parameters. In this study, Reynold Number was used for unit conversion, since if the Reynold numbers of two systems are same, then they are representing the same physics. The process of unit conversion shown below: first, the Δx can be determined by the space discretization N

$$\Delta x = \frac{L}{N} \tag{4.28}$$

After determining Δx, Δt should be choose carefully, since:

$$u_p = u_{lu}\frac{\Delta x}{\Delta t} \tag{4.29}$$

Because the speed of flow in LB model can't exceed the speed of the sound and In order to ensure the numerical stability and reduce numerical error:

$$\Delta t < \frac{\Delta x}{\sqrt{3}} \tag{4.30}$$

After discretization parameters are determined, the Reynold's Number of the system need to be calculated and based on the result, the lattice viscosity can be determined as:

$$v_{lb} = \frac{\Delta t}{\Delta x^2}\frac{1}{Re} \tag{4.31}$$

4.4. Limitation and Error of Shan-Chen Multiphase Model in Palabos

Palabos is an open-source solver based on the lattice Boltzmann method the library is a framework for general-purpose computational fluid dynamics (CFD) the library in written in C++ and has great compatibility with HPC and parallel computing. The density of two components can't be too close to each other when the Shan-Chen model in the Palabos are used. Numerical instability will occur when one fluid has density $\pm 10\%$ around another. This doesn't influence the simulations have been done in this work because the wetting phase and non-wetting phase densities are 1000kg/m^3 and 800kg/m^3 respectively, however, the mechanism of instability is unknown yet. In Shan-Chen model, the biggest limitation for multiphase simulation is that the surface tension is a fix value by the model parameters, the surface tension value in our model is $\sigma = 0.0847$. There is no limitation of viscosity ratio in Shan-Chen model, however, because of the way viscosity is set in Shan-Chen model. However, high viscosity ratio simulation is computationally expensive. the relaxation time τ is the controlling parameter of the viscosity of fluids. Relaxation time is determined by:

$$\tau = \frac{v_{lb}}{c_s^2} + 0.5 \tag{4.32}$$

In which $c_s$is the speed of sound in lattice unit which is $1/\sqrt{3}$

In Multi-Component Multiphase Shan-Chen model, the multiple relaxation times are used to specify the viscosity of each component. When the relaxation time is larger than 2, the instability issue occurs during the simulation. Therefore, the relaxation time should be kept lower than 2, which means v_{lb} should be smaller than 0.5. In Equation 4.32, the kinetic viscosity in

lattice unit is determined by Re, Δx and Δt. Since Re is fixed, smaller Δt will be used to keep the value of v_{lb}below 0.5, which means it will take more time for the simulation to finish.

CHAPTER 5. MODEL BUILDING AND METHODLOGY

5.1. Geometry of Porous Media

In this work, the porous media model used were periodic uniform random sphere pack and periodic non-uniform random sphere packs in order to investigate the impact of heterogeneity to relative permeability curves. Yade (the source codes for discreet element analysis are available on https://yade-dem.org/doc/) was used to generate the sphere packs. The uniform and non-uniform sphere packs have dimension as $4 \times 10^{-4} * 4 \times 10^{-4} * 4 \times 10^{-4}\, m$, the sphere radius in the sphere pack is 15 μm. The uniform random sphere pack consists of 1419 spheres (partial spheres included as well) and its porosity is 36.8%. The property of sphere packs is shown in Table 5.1 and Figure 5.1 shows the geometry of uniform random sphere pack.

Table 5.1. The properties of uniform and non-uniform sphere packs

	Perturbation of r	Porosity %
Uniform sphere pack	0	36.8%
Non-uniform sphere pack 1	25%	37.1%
Non-uniform sphere pack 2	50%	37.2%

5.2. Relative Permeability Calculation

Determination of relative permeability can be done either under unsteady-state and steady-state. In this work, the relative permeability curves were obtained under steady-state condition. In the LB model, the way steady-state condition is achieved by fixing the wetting phase saturation in the model and apply the same body force for each phase. The simulation will be running until the relative permeability and velocity has converged with the criterion that ε <

10−5. Later on, the wetting phase saturation will be altered in order to get the full relative permeability curve.

The relative permeability is a scaling factor which has value between 0 and 1 for each phase and its defined in terms of extension of Darcy's law:

$$k_{r,\alpha}(S_\alpha) = -\frac{v_\alpha(S_\alpha)\Delta P_0}{v_0 \Delta P(S_\alpha)} \tag{5.1}$$

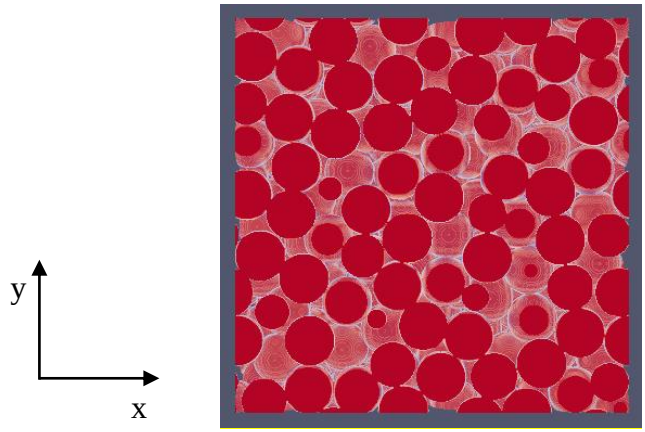

Figure 5.1. Uniform periodic random sphere pack model. The sphere pack dimension is $400\mu m$, the sphere radius in the sphere pack is $15\ \mu m$.

where α refers to the fluid phase and S_α is the phase saturation. v_α is the volumetric fluid velocity of phase α, also referred to the Darcy velocity:

$$v_\alpha = \frac{Q_\alpha}{A} n \tag{5.2}$$

Where Q_α is the flow rate of phase α and A is the cross-section area and n is the unit vector in flow direction. v_α can also be calculated by averaging local velocity over entire pore space Ramstad (2012)

$$v_\alpha = \phi \sum_x \frac{\rho_\alpha}{\rho} u \tag{5.3}$$

where ϕ is the porosity of the porous median.

5.3. Simulation Setup

5.3.1. Initial Condition and Boundary Condition of Model for Analysis of Interface Instability

The uniform random periodic sphere pack is used as porous media for this set of simulations. The periodicity of the sphere pack will eliminate boundary effect. The initial state of the model is shown in Figure 5.2. The red phase is wetting phase and blue phase is non-wetting phase. At the beginning of simulation, the left side of the model is filled with wetting phase and the rest of the pore space is filled with non-wetting phase. The wetting phase saturation of the model is 41% which was determined by using the number of the blocks occupied by wetting phase over total pore volume. In x direction, periodic boundary with pressure gradient was set, Δp between left boundary and right boundary in physical unit is 0.05 psi. in y and z direction, the periodic boundary condition is applied.

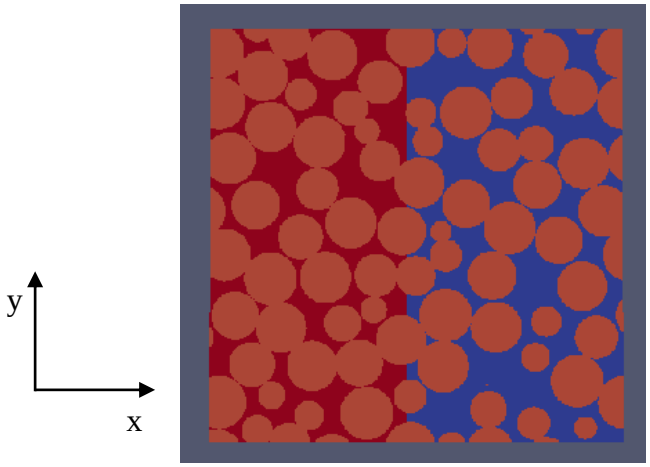

Figure 5.2. The center sliced view of initial condition of the model (z=200)

Three (3) sets of simulations were designed in order to show the interfacial instabilities caused by viscous force and capillary force. The general parameters of the model are shown in Table 5.2 and the fluid properties are shown in Table 5.3.

The general parameters of the model include Δx, Δt, fictitious density (controlling the wettability) and the G value of the model. G value controls the strength of interaction between phases. In order to ensure the numerical stability of the model the value of Δx, Δt and G should be carefully chosen. The higher G value is, the shaper the interface is. However, the high G value will cause numerical instability.

Table 5.2. The general input data of the LBM model

Δx	2.5E-3
Δt	2.5E-9
G	0.8
Contact angle (degrees)	50

With the viscous ratio and the capillary number of the simulations, the red dots in Figure 5.3 (the phase diagram developed by Lenormand (1988)) show the state of three simulations.

Table 5.3. The fluid properties of each set of simulation

	Simulation 1	Simulation 2	Simulation 3
Non-wetting phase viscosity(cp)	100	100	100
Wetting phase viscosity(cp)	1	100	450
Viscosity ratio (μ_w/μ_n)	0.01	1	4.5
Capillary number (Ca)	0.016	0.0451	0.1691

Capillary Number $Ca = \frac{v\rho V}{\gamma}$ where v is the average viscosity of fluid, ρ is average density of fluids, V is the flow velocity and γ is surface tension. Simulation 1 is on the boundary of the viscous fingering and simulation 2 and 3 are in the transition zone. Here need to be noted

that the phase diagram developed by Lenormand (1988) was for uniform porous media. For different porous media, different phase diagram need to be adapted. Therefore, the diagram here just to show the relationship between viscosity ratios and capillary number of designed simulations.

5.3.2. Initial and Boundary Condition of Models

In order to investigate how heterogeneity affects relative permeability curves, three sphere packs (uniform and non-uniform sphere packs mentioned earlier) were placed serially,

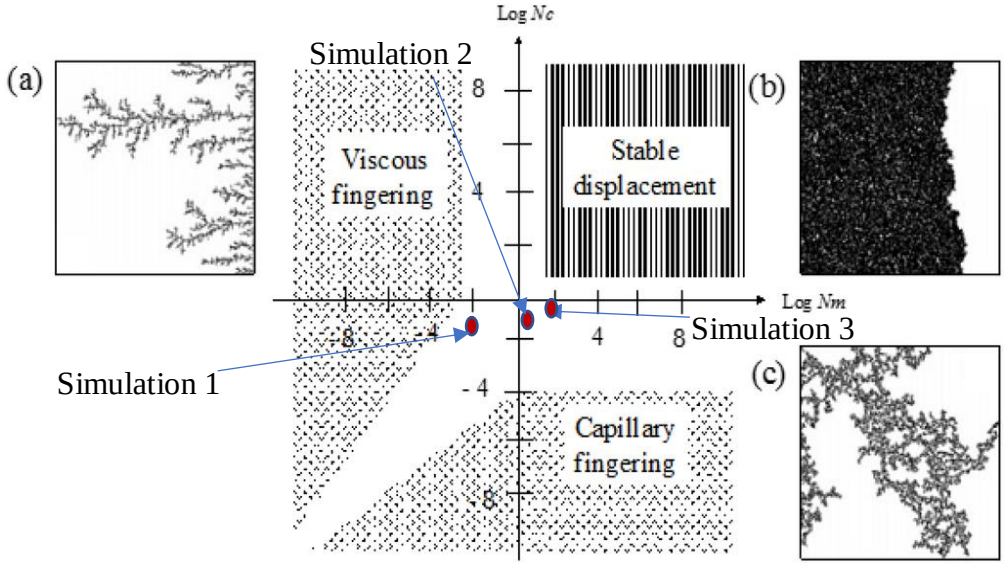

Figure 5.3. Phase diagram by Lenormand (1988), the red dots in the diagram show the state of three simulations

and right boundary in physical unit is 0.15 psi. in y and z direction, the periodic boundary condition is applied.

Five simulations with the wetting phase saturation as 10%, 25%, 50%, 75% and 90% were done and simulations were running till the steady state (relative permeability value

perturbation ε < 10−5) was reached, the relative permeability can be calculated at each saturation point so that the full relative permeability function can be obtained.

Table 5.4. Input data of model of investigating effect of heterogeneity on relative permeability curves

Δx	2.5E-3
Δt	2.5E-9
G	0.8
Contact angle (degrees)	50
Non-wetting phase viscosity(cp)	80
Wetting phase viscosity(cp)	8

The input data of the simulations are shown in Table 5.4. shown in Figure 5.4. The model consists of 1200*400*400 blocks, in x direction, periodic boundary with pressure gradient was set, Δp between left boundary.

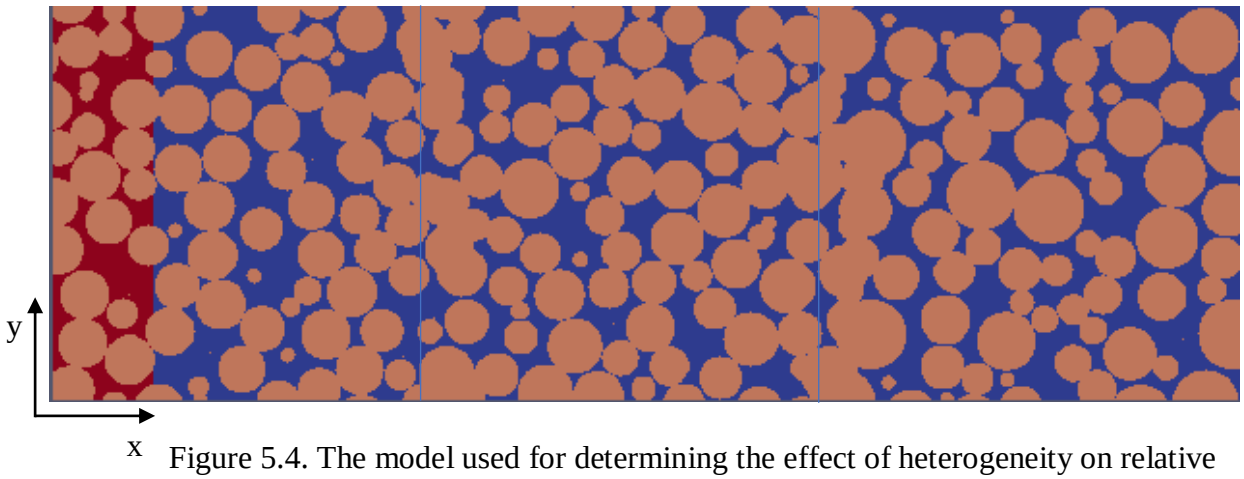

Figure 5.4. The model used for determining the effect of heterogeneity on relative permeability

CHAPTER 6. RESULTS AND DISCUSSIONS

6.1. Simulation Performance and Running Time

The LBM simulations were performed using LSU-HPC on QueenBee2 from LONI system. Palabos models work well with HPC and these parallel simulations run efficiently with 80 cores. Typical wall clock time taken to reach steady state for permeability calculation is around 49 hours.

6.2. Model Verification

A few verification tests are presented here to demonstrate the capability of LBM Shan-Chen model to capture the underlying multiphase flow physics in simpler geometries.

6.2.1. Laplace Test and Surface Tension

The surface tension in Shan-Chen model is not a specified pressure tensor instead Shan-Chen model uses a body force to implement the surface tension. The value of surface tension is controlled by the higher order term from applying Taylor expansion to force mentioned in Equation 4.26 which is $\frac{G}{18}\psi\nabla\Delta\psi$. It can be seen that the surface tension is controlled by *G* value, but the value of surface tension need to be determined by performing Laplace test.

Based on Laplace law $\Delta p = \frac{2\gamma}{R}$, the simulation was designed in the way that there are a series of droplets with different sizes in another immiscible fluid with no external force. When the simulation reaches equilibrium state, the radius of droplet and the pressure difference between inside of the bubble and outside of the bubble can be determined. Then the data are

plotted in Figure 6.1, the result of LB simulation shows great agreement with Laplace law and the slope is the value of surface tension which is: 0.0847 in lattice unit

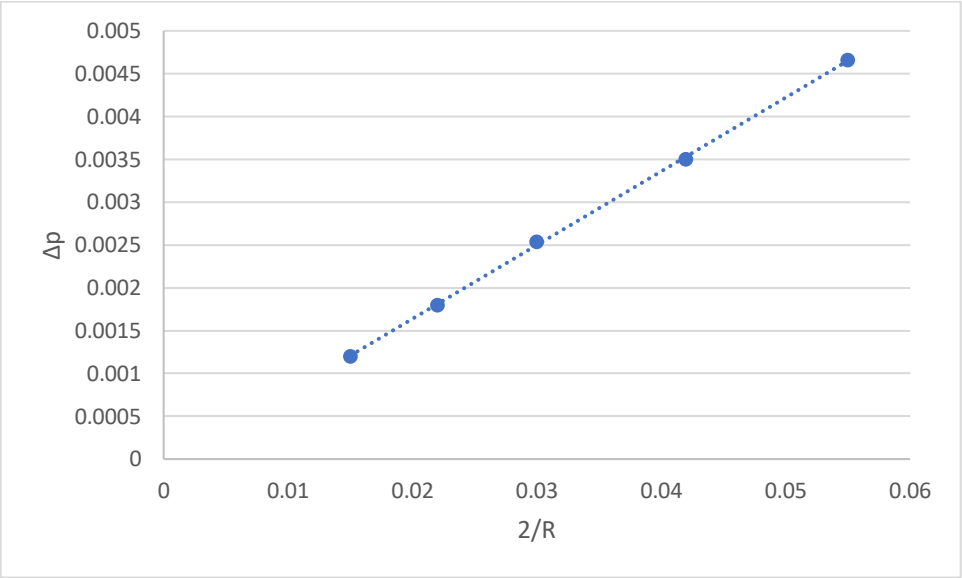

Figure 6.1. The result of Laplace Test, the result of LB simulation shows great agreement with Laplace law and the slope of the straight line is the value of surface tension.

6.2.2. Verification of Contact Angle Implementation

In order to show the implementation of contact angle in Shan-Chen model, three simulations have been done. The contact angle between fluid and solid surface in Shan-Chen model is controlled by fictitious density of the surface and the density of fluid. When the value fictitious density of the solid surface is close to one fluid, the surface will show more attractions to one fluid and show less attraction to the other fluid.

The simulation is designed in the way that a drop of red fluid whose density is 1 is placed above the surface. The model is filled with blue fluid whose density was set as 0.1. When the fictitious density of the surface is set to be 0.55 which is the average of fluid densities, the

contact angle of 90 degree is expected. After starting the simulation, due to the surface tension and attraction of surface to the fluids, the fluid start wetting the surface and maintain the minimum surface area, as the equilibrium state is reached, the contact angle is 90 degrees which is shown in Figure 6.2.

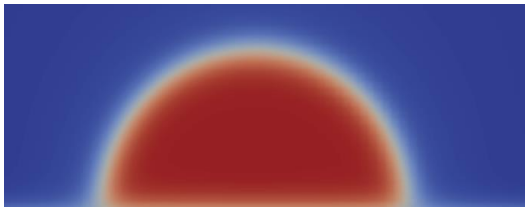

Figure 6.2. 90-degree contact angle when the fictitious density is set as the average density of two fluids

Later on, the fictitious density of the surface was set to be 0.3, the blue fluid is more attracted to the surface and the contact angle for red fluid is expected to be 130 degrees. The simulation result which is illustrated in Figure 6.3 shows the same contact angle as we expected.

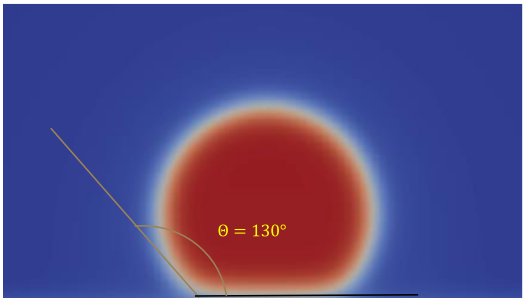

Figure 6.3. 130-degree contact angle when the fictitious density is set as the 0.3

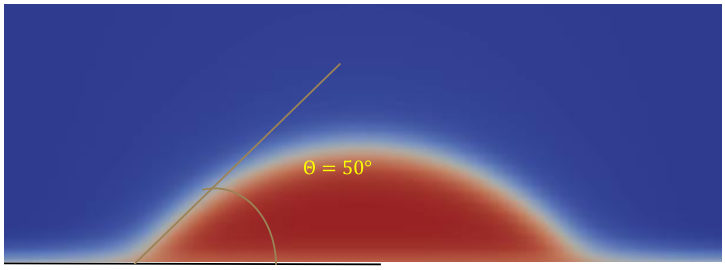

Figure 6.4. 50-degree contact angle when the fictitious density is set as the 0.8

Figure 6.4 shows the when the fictitious density is 0.8, the contact angle is 50 degrees.

6.2.3. Permeability Calculation

The permeability of close packed spheres has been extensively studied because it is one of the basic models of porous media. Multiple formulas have been proposed for permeability of sphere packs. The Kozeny−Carman correlation (1995) has been widely accepted in industrial applications for permeability estimation. He predicts that:

$$K = \frac{\varepsilon^3}{36k(1-\varepsilon)^2} d^2 \tag{6.1}$$

K – permeability (m2)

E – porosity (dimensionless)

d – sphere diameter (m)

k – Kozeny-Carman constant, k = 5 for beds packed with spherical particles

Based on the correlation, the absolute permeability of our uniform random sphere pack is 432md the calculated permeability by using single phase LBM simulation is 468md which quantitatively agrees with the permeability value predicted by Carman-Kozeny model.

6.3. Grid Independence Test

The independence grid test was performed to determine what is the optimum mesh should be used in LBM simulations in this study. The numerical model for grid independence test whose boundary condition is periodic boundary condition in *x, y* and *z* directions with pressure gradient in *x* direction. The meshes used for independence grid test are 300*300*300 (coarse mesh), 400*400*400 (medium mesh) and 500*500*500 (fine mesh), the model is shown

in Figure 6.5. the parameters compared is the average velocity of the wetting phase. Three simulations were done in the multiphase fluid flow in model shown below, Input data of the simulation is shown in Table 6.1. The result of independence grid test shows that there is 20% of different of average wetting phase velocity between coarse mesh and medium mesh and only 7% difference between medium mesh and fine mesh. Because the fine mesh is computationally expensive, therefore medium mesh was used for simulations.

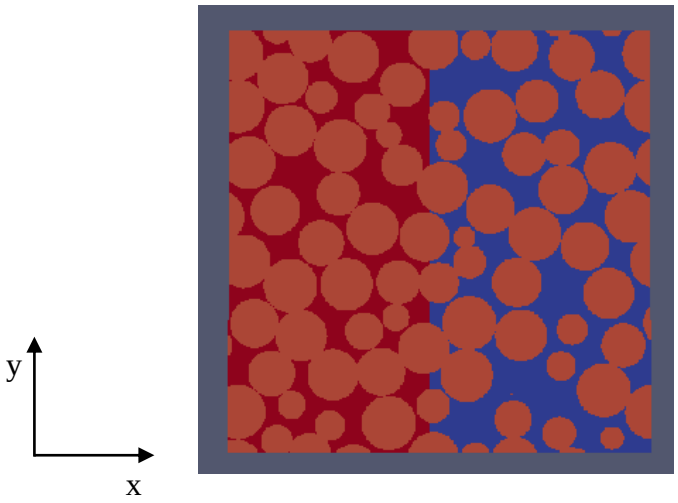

Figure 6.5. Uniform periodic random sphere pack model used for independence grid test. The sphere pack dimension is $400\ \mu m$, the sphere radius in the sphere pack is $15\ \mu m$.

Table 6. 1. The input data of grid independence test

Δx	2.5E-3
Δt	2.5E-9
G	0.8
Contact angle (degrees)	50
Non-wetting phase viscosity(cp)	80
Wetting phase viscosity(cp)	8
Δp(psi)	0.05

6.4. Interfacial Instabilities in Pore-Scale

6.4.1. Viscous Fingering in Pore-Scale

When the viscosity ratio (the ratio of viscosity of displacing fluid and displaced fluid) is set as M=0.01, due to the pressure gradient in *x* direction, the fluid starts to flow. The phase distribution at different time steps is shown below in the Figure 6.7 and Figure 6.8. In Figure 6.7, the sharp finger-shaped interface in large pore space is indicated by yellow arrows. Since the wetting phase viscosity is much lower than that of the non-wetting phase, the wetting phase flows favorably under pressure gradient and as soon as the interface encounters the pore throat to pore space entrance (expansion), the fluid viscosity difference favors the wetting phase to penetrate through the pore space instead of forcing the flow along the grain surface.

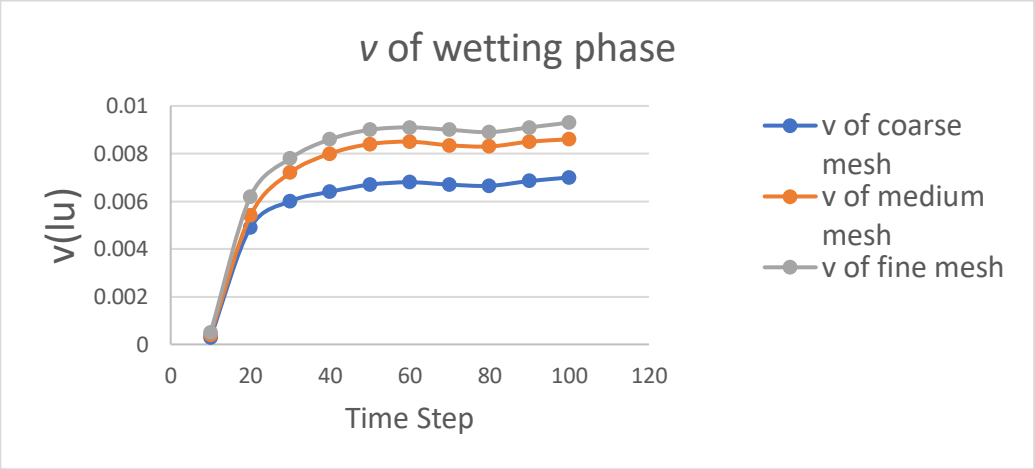

Figure 6.6. the fluid average velocity changing with time in simulation with coarse, medium and fine mesh.

In this simulation, the viscous force is much higher than the capillary force. When the aspect ratio of pore is not changing dramatically, the wetting phase flows along grain surface and spreads over the grain surface due to the capillary force. The distribution of wetting phase in

pore-scale has three forms which are: film around grain surface, bridge between grains and lake in the pore space and they are all shown in Figure 6.7. In addition, the wetting phase in the green circle is discontinued from the other parts of the wetting phase, because the wetting phase could not bear steer stress. In the surface view of the simulation model (Z=0 plane), the viscous fingers are more visible and the finger shaped interface is shown more apparently in Figure 6.8. The interface in the pore space is very pointy. The area within the black circle, the wetting phase is discontinued from the other part of the wetting phase due to low wetting phase viscosity and the wetting phase spread out and becomes thin films around grain surface due to capillary force. The circles with letter "V" show the front position of wetting phase. In addition, the lake, film and bridges can be observed in Figure 6.8 as well.

6.4.2. Capillary Fingering in Pore-Scale

When the viscosity ratio of non-wetting phase and wetting phase is M=1, the influence of viscous force imbalance can be eliminated. However, the resulting interface displacement process might not be stable. Capillary forces can result in interfacial instability since the grain surface have different affinity towards the wetting and non-wetting phase.

Two displacement mechanisms were observed in the pore-scale in capillary fingering:

1. Piston displacement
2. Film displacement

Piston shaped displacement happens when the non-wetting phase can flow out the pore space as continuous phase and the piston shape of interface shows up between wetting phase and non-wetting phase.

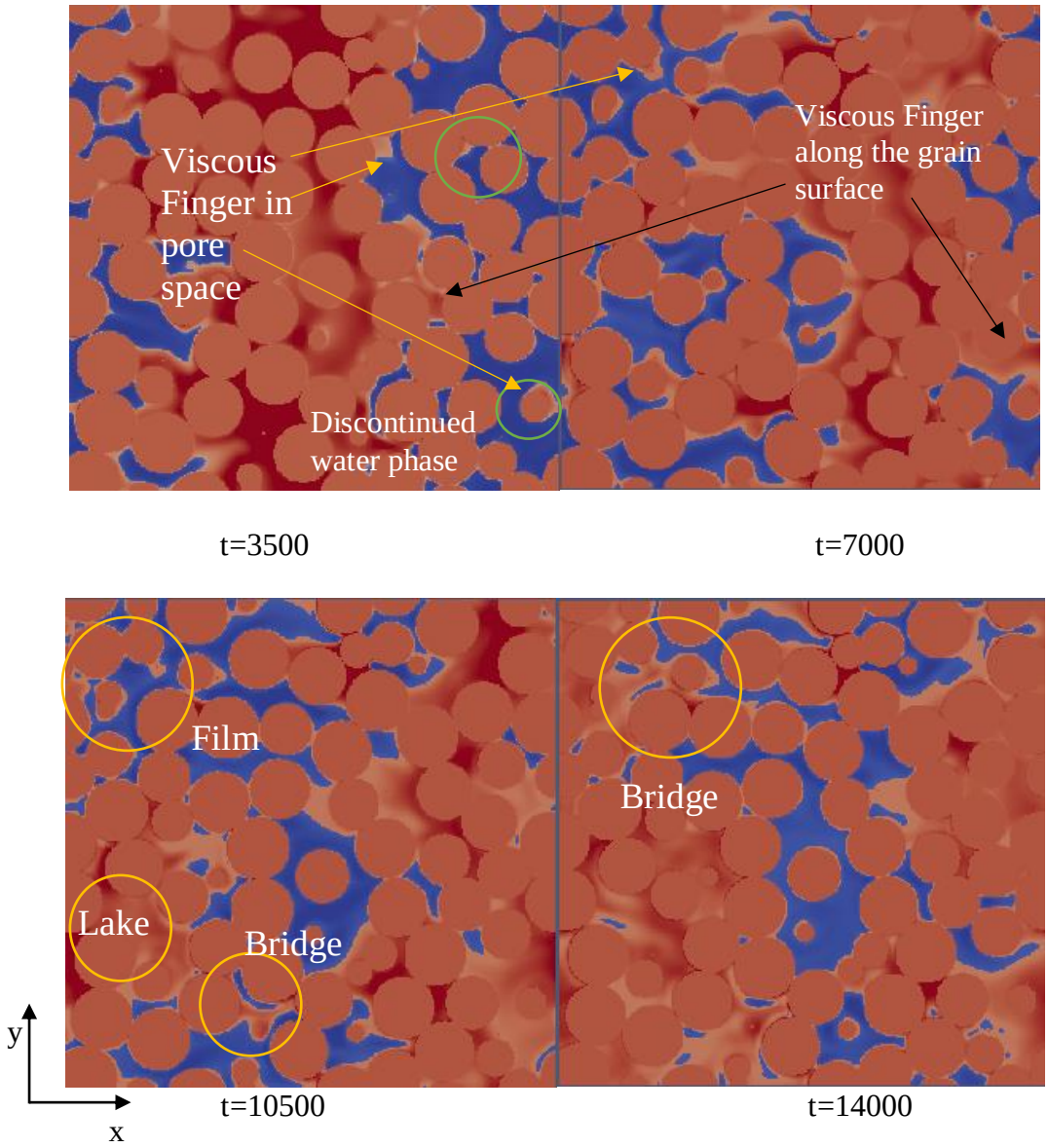

Figure 6.7. Sliced view of the center of the model (z=200), the viscous fingers are noted by yellow and black arrows. The yollow circles show the distribution of wetting phase

It happens when the interface met pore throat and then enter pore space, the interface could not maintain stable, and will jump rapidly to evolve a new stable interface, the process is called “Haines Jump”. This phenomenon has been observed in the pore-scale LBM simulation in this study.

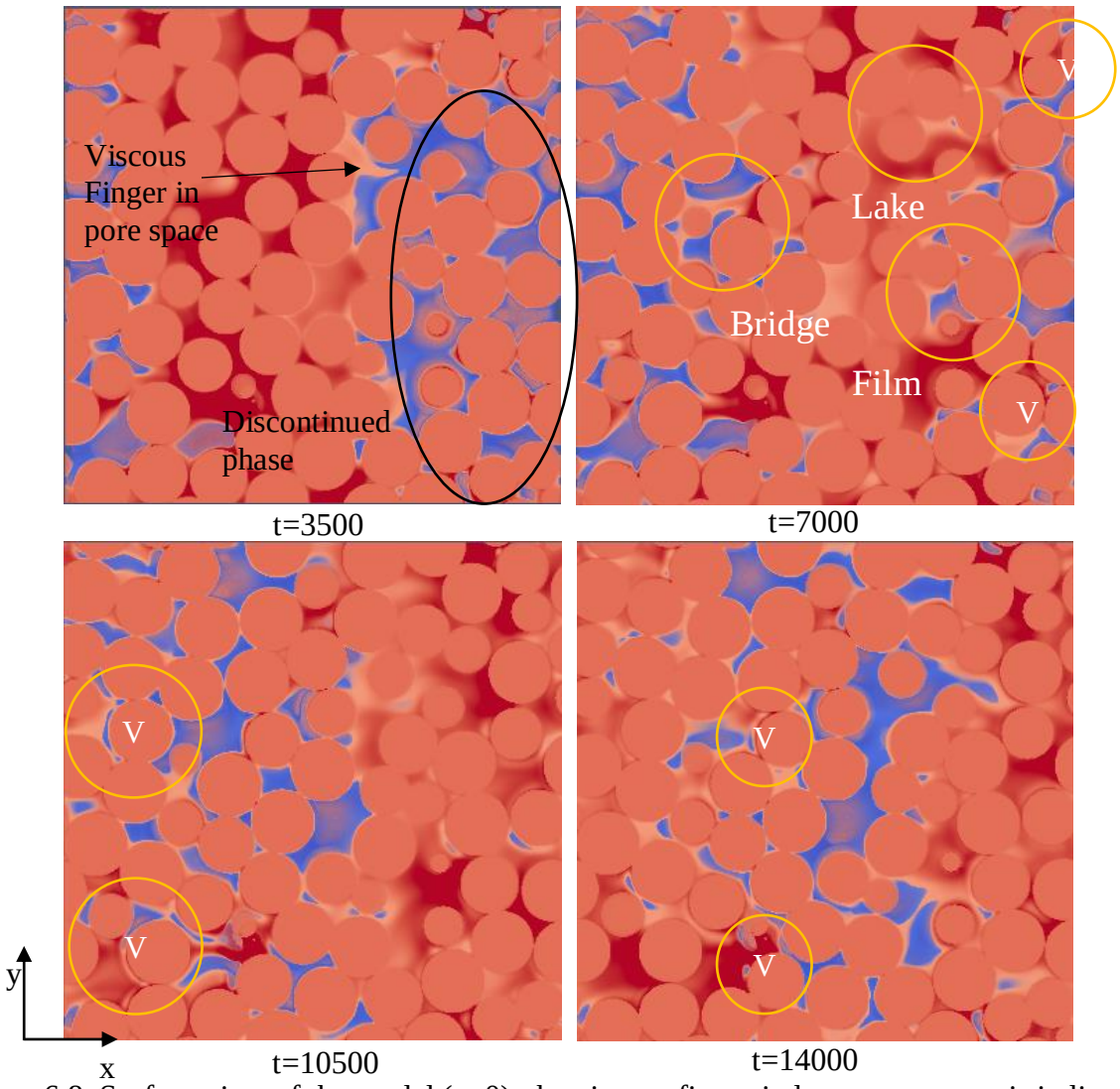

Figure 6.8. Surface view of the model (z=0), the viscous finger in large pore space is indicated by black arrow and the discontinued wetting phase is shown in black circles

The area within black circles in Figure 6.10 is large pore space in the model. At time step t=3500, the pore is filled with non-wetting phase, as the wetting phase enters into the large pore space, the interface becomes unstable, the interface jumps and reach the new stable state. At the same time, the non-wetting phase was displaced very fast and then the opening of the pore space between grains are blocked by the wetting phase due to the wetting phase got pulled in to small pores by capillary force. Then the non-wetting phase remained in the pore space is gradually

being displaced by wetting phase film flow around the grain surface. The process shows that the bulk flow goes faster than the film flow.

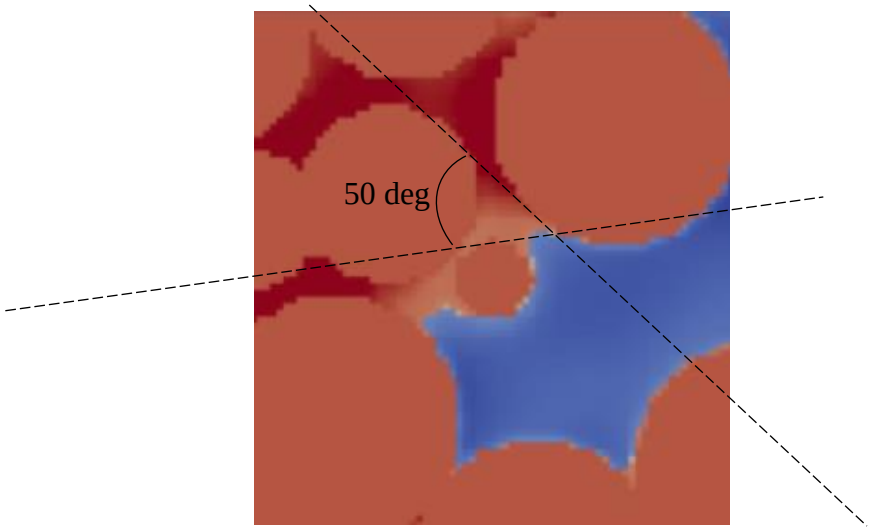

Figure 6.9. Illustrating advancing contact angle of wetting phase in simulation results ~ 50 degrees (same as the value set in the input parameters)

Film displacement happens when the displacing fluid encounters the pore throat and pore space because of capillary entry pressure and the shape of interface, the fluid flow along the surface of the grain and gradually displaces the non-wetting phase.

In Figure 6.11, the pore space indicated in black circle shows the film displacement. The wetting phase went into the pore space by means of film and the non-wetting phase is surrounded by film of wetting phase, then the non-wetting phase was fully displaced by the wetting phase with film flow as t=7000. In surface view of the model Figure 6.12, the feature of capillary fingering was shown more clearly, the capillary finger in area indicated by black circles shows clearer piston shaped displacement and area within green circles show the phenomenon of film displacement. The circles with letter “C” shows the frontal of capillary fingers. When the viscous ratio (the ratio of viscosity of displacing fluid and displaced fluid) is M=4.5, the displacement

process is compared with the displacement process of M=1. The flow pattern of M=1 and M=4.5 are identical to each other, however there are some small differences.

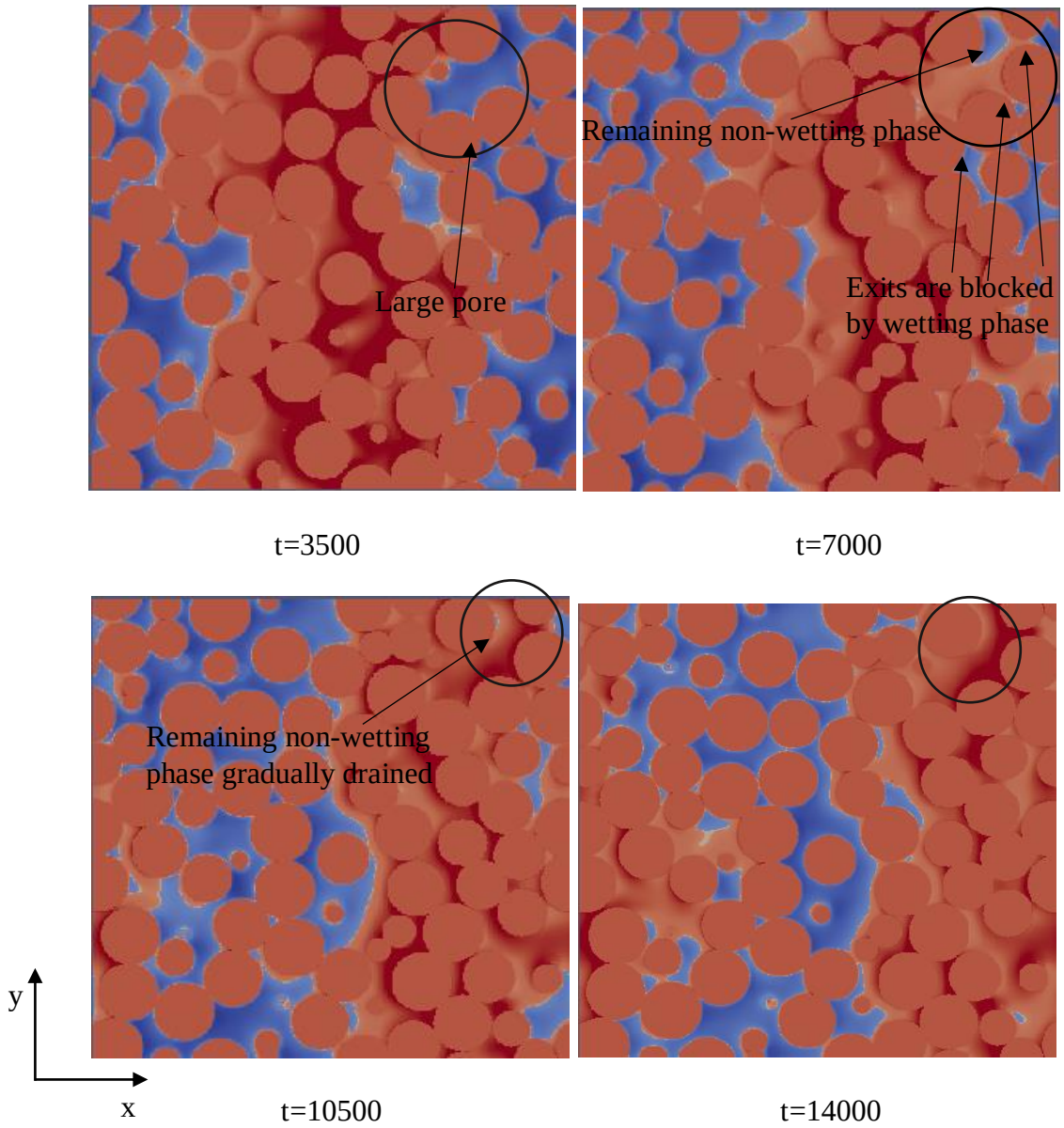

Figure 6.10. Sliced view of the center of the model of M=1 (z=200). The process of piston like displacement is shown. In the figure, wetting phase is red and non-wetting phase is blue

In surface view of the model Figure 6.12, the feature of capillary fingering was shown more clearly, the capillary finger in area indicated by black circles shows clearer piston shaped displacement and area within green circles show the phenomenon of film displacement. The

circles with letter “C” shows the frontal of capillary fingers. When the viscous ratio (the ratio of viscosity of displacing fluid and displaced fluid) is M=4.5, the displacement process is compared with the displacement process of M=1. The flow pattern of M=1 and M=4.5 are identical to each other, however there are some small differences. In Figure 6.13 a) the area within the black circles, they are the same pore space in the model, the displacement mechanism is both film displacement and the interface look identical, however, the speed of film flow is higher when M=4.5.

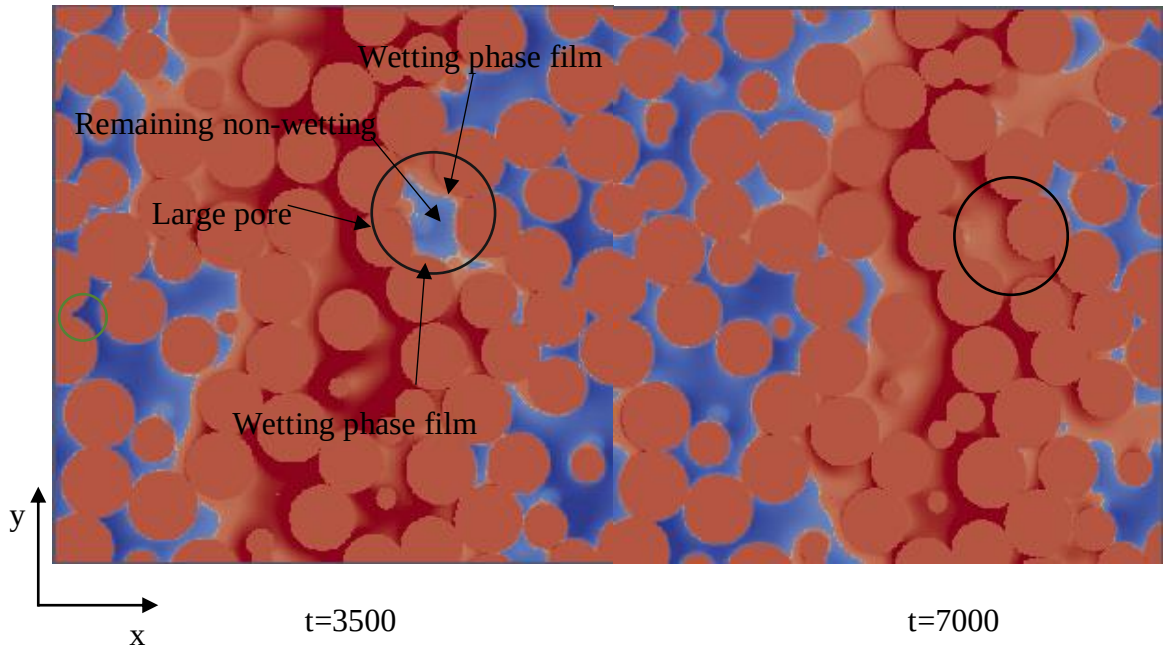

Figure 6.11. Sliced view of the center of the model of M=1 (z=200), the film displacement process was shown, wetting phase is red and non-wetting phase is blue

In Figure 6.13 b), the shape of remaining non-wetting phase in black circles when M=4.5 is longer in x direction and narrower in y direction which is caused by the film flow, which means when M=4.5 the film flow moves faster than the film flow when M=1. The volume of remaining non-wetting phase in the pore-space in Figure 6.13 c) shows the same phenomena.

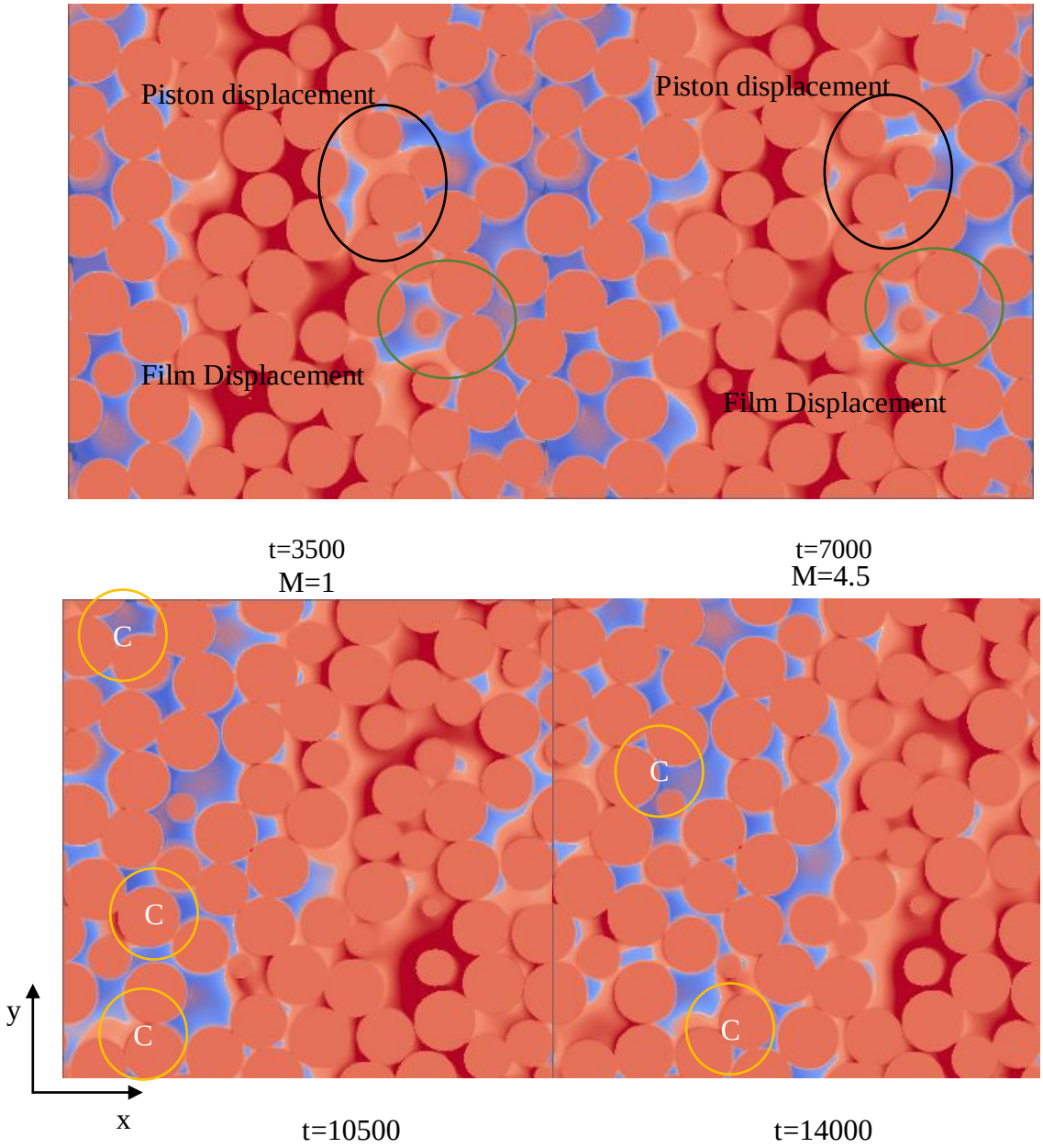

Figure 6.12. Surface view of the model (z=0) of M=1, the piston like displacement process is shown in black circles and the film displacement is shown in green circles

6.4.3. Comparison of Viscous Fingering and Capillary Fingering

In order to compare the difference between interface of viscous fingering and capillary fingering in pore scale, the 3D iso-surfaces of the wetting phase was generated and shown in Figure 6.14. In the figure, the red circles indicated the frontal of the wetting phase.

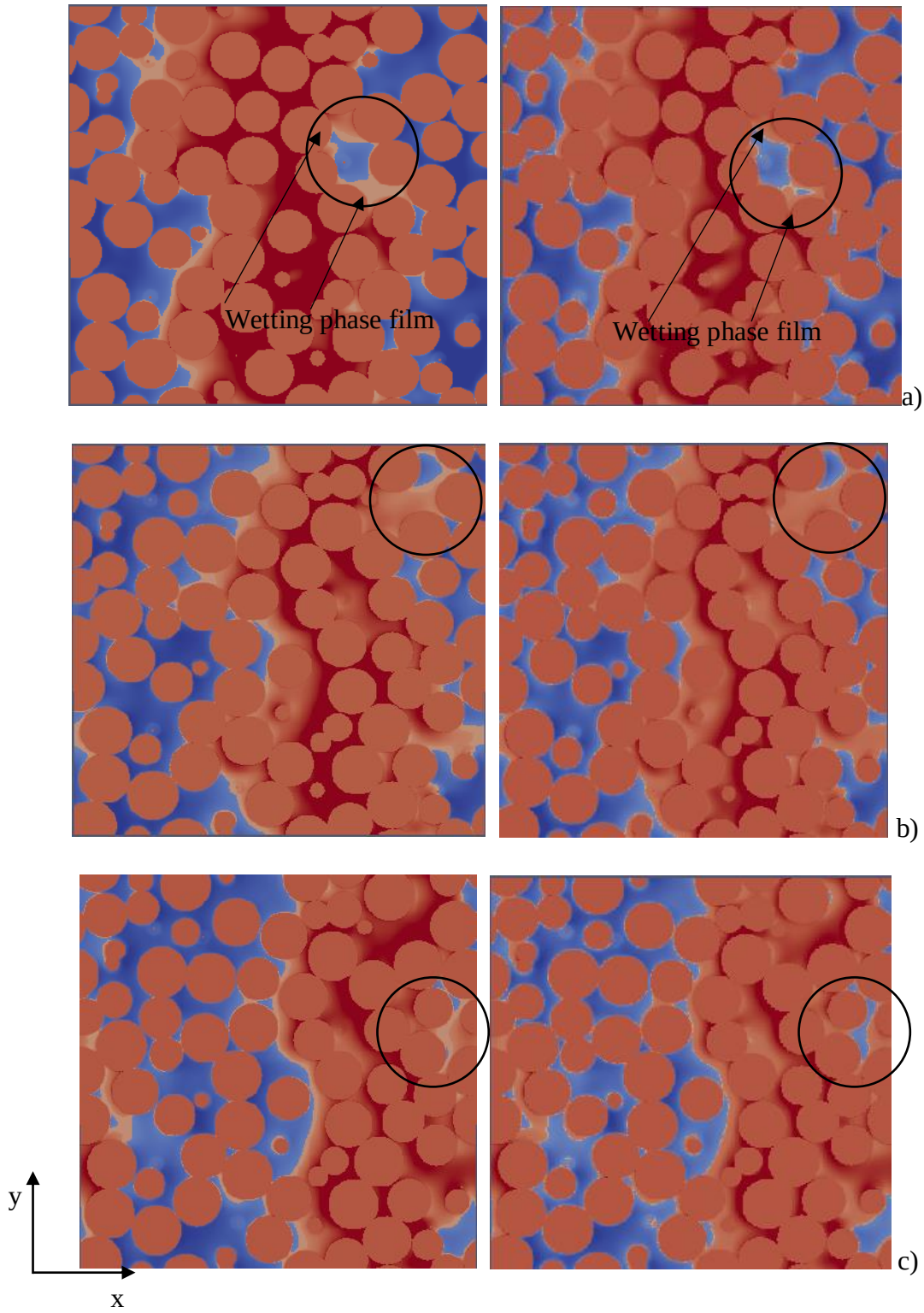

Figure 6.13. The comparison of M=1 and M=4.5. Sliced view of the center of the model (z=200), The displacement of capillary fingering with different viscosity ratio is compared

When the wetting phase viscosity is 1% of the non-wetting phase viscosity, the wetting phase is much more mobile than non-wetting phase. the interface is very unstable, and the wetting phase tend to shoot through pore space freely. However, when M=4.5, the displacement process is controlled by capillary force, therefore the wetting phase mainly flow along the grain surface. This is why when compared with M=0.01, the interface of M=4.5 is mainly sphere-shaped interfaces which are the interfaces between wetting phase and grain surface. Therefore, in case of M=0.01, the fluid flow was mainly influenced by viscous force which means the structure of pore space controls the flow pattern and only a few sphere-shaped interfaces can be seen, however when M=4.5, the fluid flow is controlled by the structure of pore throat due to capillary force.

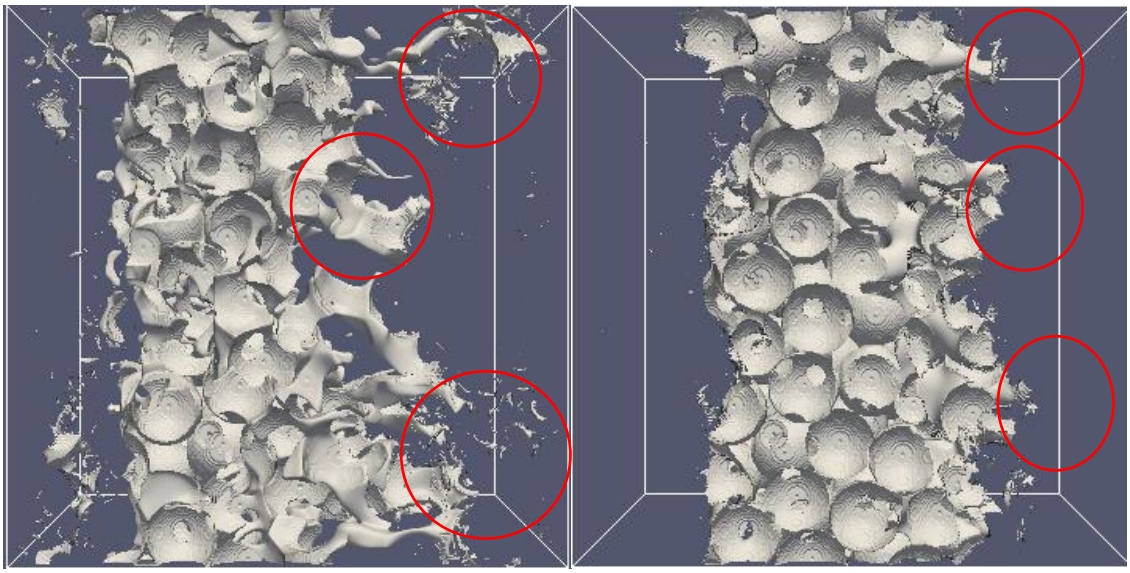

M=0.01 M=4.5

Figure 6.14. the isosurface of wetting phase, on the left side, the viscosity ratio is 0.01, on the right side the viscosity ratio is 4.5

Figure 6.15 is the surface view of the model with different viscosity ratio at same time step(t=7000), the area indicated by black circles shows how the interface looks like when it

encounters the same pore structure, In the case of M=0.01 the interface of wetting phase is pointy in the pore space and it is very different from case of M=1 and M=4.5. What happened was while the wetting phase is moving, because of the attraction force from the solid surface, the wetting phase migrate along the surface instead of shoot through in the pore space of the model when M=0.01. At the same time, the phase distribution of M=1 and M=4.5 are very similar, However, by looking at the displacement within the black circle, it can be seen that the film flow has higher speed in the case of M=4.5 than M=1. The area within the blue circles shows that the flow pattern of viscous fingering and capillary fingering are different in the same porous media. The pore space is occupied by wetting phase when M=0.01, however, the same pore space was occupied by non-wetting phase in the cases of M=1 and M=4.5. In addition, the small pores within the green circles of case M=1 and M=4.5 are occupied by wetting phase due to capillary force, however, in the case of M=0.01, the small pores are occupied by non-wetting phase since the viscous force is dominate force.

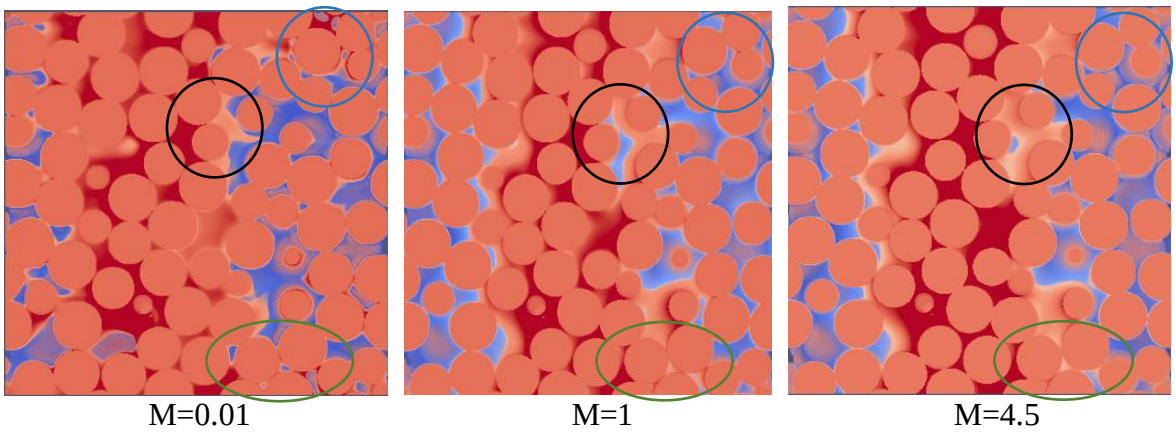

Figure 6.15. Surface view of the models (z=0) of M=0.01, M=1 and M=4.5. The flow patterns and interfaces are different for viscous fingering and capillary fingering in pore-scale.

6.5. Relative Permeability Curves.

6.5.1. Relative Permeability in Sphere Packs

In order to obtain the relative permeability curves for imbibition process, the wetting phase saturation is fix at points: 0.1, 0.25, 0.5, 0.75, 0.9, the simulation is running till it reaches steady-state condition. The steady-state criterion is the change of relative permeability ε is smaller than 10^{-5}. The relative permeability functions for irregular arrangement of uniform diameter sphere packs from the simulation are shown below in Figure 6.16.

With the method which the saturation is fixed in one simulation and the simulation is ran till steady state condition used to determine the relative permeability values, the residual non-wetting saturation and irreducible wetting phase saturation can't be determined. Therefore, the results at $S_w = 0.1$ and S_w=0.9 might not have actual physical meaning. The results of relative permeability curves from the simulation, the interception of wetting phase and non-wetting phase relative permeability curves is around 0.64.

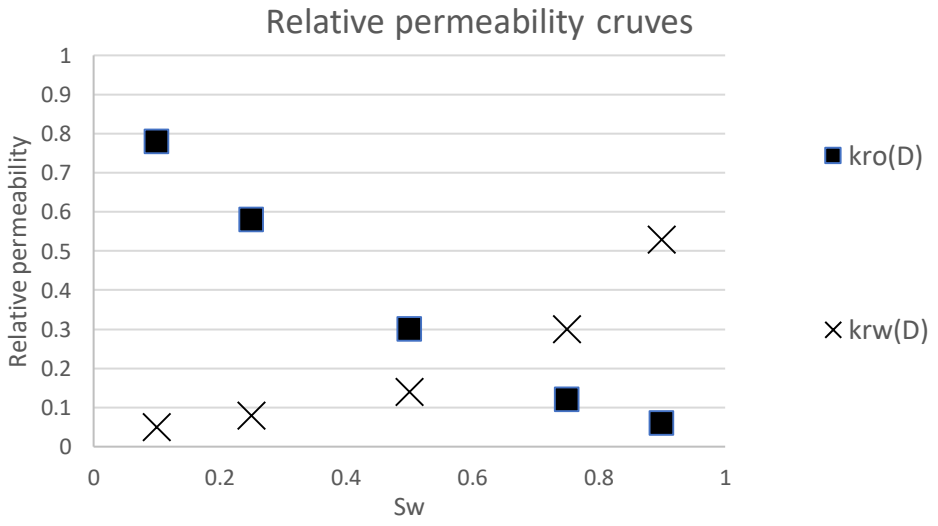

Figure 6.16. Relative permeability in uniform sphere packs for wetting and non-wetting phase

6.5.2. Impact of Heterogeneity on Relative Permeability Curves

The same method that has been used to determine the relative permeability curves in previous part has been used in this for each sphere pack and the average relative permeability of the whole model. The results are shown in figure below. From the results, for imbibition process, the relative permeability of non-wetting phase in the uniform sphere pack is higher than Non-uniform sphere packs. However, for wetting phase, the relative permeability in non-uniform sphere packs are slightly higher than in uniform sphere pack. In addition, the poor the sorting is, the lower relative phase permeability is for non-wetting phase, as for as wetting phase the trend is opposite.

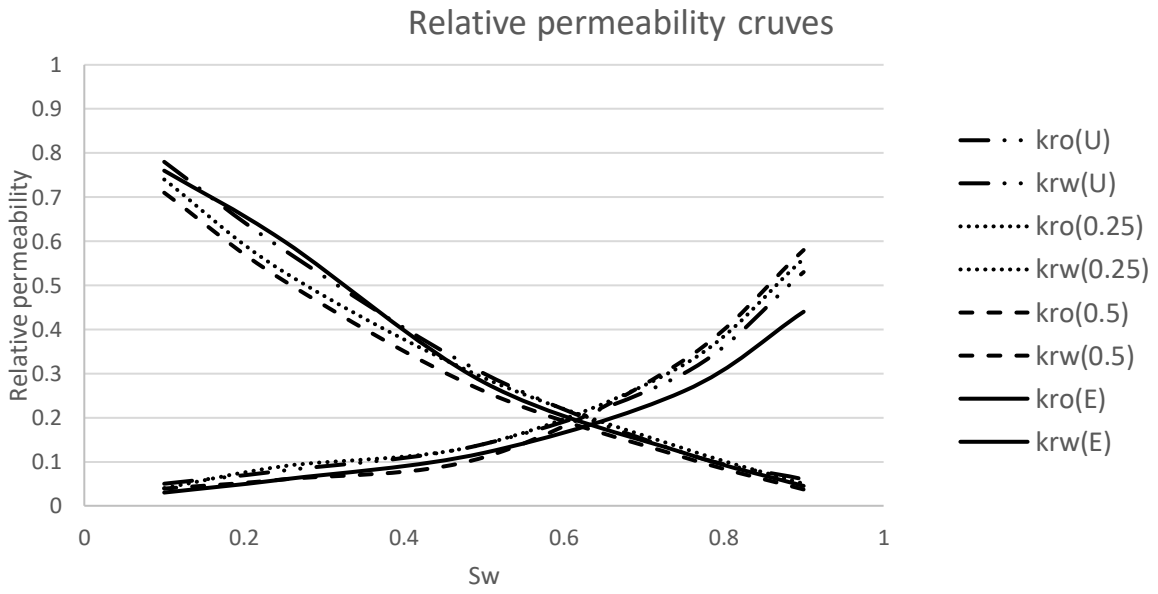

Figure 6.17. Relative permeability functions in uniform sphere pack and Non-uniform sphere packs and the effective relative permeability.

As far as effective relative permeability, for non-wetting phase, the effective permeability is very close to the relative permeability of uniform random sphere pack, which means the heterogeneity doesn't greatly affect relative permeability function for non-wetting phase. But for wetting phase the heterogeneity has great negative effect on the relative permeability function.

However, the relative permeability curves are directly related to the pore structure, so this trend might not apply for all the porous media.

Chapter 7. CONCLUSIONS

Two main objectives of this thesis are to:

1. Visualize and analyze the two different interfacial instability mechanisms and their fluid flow structure at the pore-scale resolution;
2. Investigate how heterogeneity could impact the relative permeability curves.

Results of the pore-scale simulation done by using LBM Shan-Chen multiphase model shows the following facts:

- Shan-Chen model can be used to simulate multiphase flow in pore-scale and phenomenon of capillary fingering and viscous fingering in pore-scale were shown.
- When it comes to interfacial instabilities of two immiscible fluid, during immiscible flooding process, the causes of instabilities are viscous force and capillary force. Under domination of different forces, the flow patterns are different. The main difference between the viscous fingering and capillary fingering in pore scale is that: viscous fingers appear in the pore space and along the grain surface, the shape of the finger in the pore space is very pointing. However capillary fingering usually appears along the surface of the grain and the shape of the finger is controlled by the pore structure.
- Two displacement processes (piston displacement and film displacement) have been observed in the simulations and the result shows that both displacement processes happen together, and the film flow moves slower than the bulk flow. In addition, with the increase of viscous ratio, the speed of film increases.

- As far as the influence of heterogeneity on relative permeability functions, in imbibition process, the effective relative permeability was affected (lowered) by the heterogeneity for wetting phase, however, for non-wetting phase the effective relative permeability value is not greatly altered by heterogeneity.

REFERENCES

Ben-Jacob, E., Garik, P. (1990). The formation of patterns in non-equilibrium growth. Nature 343, 523–530

Blunt, M.J., Jackson, M.D., Piri, M., Valvatne, P.H. (2002). Detailed physics, predictive capabilities and macroscopic consequences for pore-network models of multiphase flow. Adv. Water Resour. 25, 1069–1089

Blunt, M.J. (2017). Multiphase Flow in Permeable Media – A Pore-Scale Perspective, Cambridge University Press. ISBN 978-1-107-09346-1.

Chuoke, R.L., van Meurs, P., Van der Poel, C. (1959). The instability of slow, immiscible, viscous liquid-liquid displacements in permeable media. Trans. AIME 216, 188–194

C. Pan. (2003). PhD thesis. University of North Carolina, Chapel Hill, USA.

Chukwudozie, C., Tyagi, M., 2013. Pore scale inertial flow simulations in 3-d smooth and rough sphere packs using lattice Boltzmann method. AIChE J. 59 (12), 2011

Chen, W 2011, Lattice Boltzmann simulation of immiscible two-phase flow at the pore scale, Thesis, United States.

Dong, B., Yan, Y.Y., Li, W.Z. (2011). Transp Porous Med 88: 293. https://doi.org/10.1007/s11242-011-9740-y

D Wilkinson and J F Willemsen (1983) J. Phys. A: Math. Gen. 16 3365

Degruyter, W., Burgisser, A., Bachmann, O., Malaspinas, O. (2010). Synchrotron X-ray microtomography and lattice Boltzmann simulations of gas flow through volcanic pumices. Geosphere 6 (5), 470–481.

D. A. Wolf-Gladrow. (2000). Lattice gas cellular automata and lattice Boltzmann models

Edo S. Boek and Maddalena Venturoli (2010). Lattice-Boltzmann studies of fluid flow in porous media with realistic rock geometries Computers and Mathematics with Applications, Volume 59, Issue 7, April 2010, Pages 2305-2314

F. H. Harlow and J. E. Welch, (1965). Phys. Fluids, 8, 2182.

G. A. Bird. (1994). Molecular Gas Dynamics and the Direct Simulation of Gas Flows, Clarendon, Oxford.

Gunde AC, Mitra SK, Babadagli T. (2010) Pore Scale Simulation of Two-Phase Fluid Flow in Berea Sandstone Core Using Lattice Boltzmann Method. ASME. International Conference on Nanochannels, Microchannels, and Minichannels.

Genty, A., Pot, V. Transp Porous Med (2013) 96: 271. https://doi.org/10.1007/s11242-012-0087-9

Hilpert, M., Glantz, R., Miller, C.T. (2003) Transport in Porous Media

Hill, S. (1952). Channeling in packed columns. Chem. Eng. Sci. 1, 247–253

Hui, M.H., Blunt, M.J. (2000). Pore-scale modeling of three-phase flow and the effects of wettability, 2000SPE/DOE improved oil recovery symposium, Tulsa, Oklahoma, 3–5 April

Holtzman (2016) Effects of Pore-Scale Disorder on Fluid Displacement in Partially-Wettable Porous Media, Scientific Reports 6, article number 36221.

Jiang, Z., Wu, K., Couples, G., van Dijke, M.I.J., Sorbie, K.S., Ma, J. (2015). Efficient extraction of networks from three-dimensional porous media. Water Resour. Res. 43, W12S03

Jin, G., T. W. Patzek, and D. B. Silin. (2004) "Direct prediction of the absolute permeability of unconsolidated and consolidated reservoir rock." SPE, no. 90084.

J. A. Sethian. (1996). Level Set Methods: Evolving Interfaces in Geometry, Fluid Mechanics, Computer Vision, and Materials Science, Cambridge University Press.

Kovscek A. (2013). Pore-scale evaluation of polymers displacing viscous oil-computational-fluid-dynamics simulation of micromodel experiments. Spe Reservoir Evaluation and Engineering;16: 144–154.

Kaviany, M. (1995). Principles of Heat Transfer in Porous Media (2nd ed.). New York: Springer.

Lenormand, R., Touboul, E., Zarcone, C. (1988). Numerical models and experiments on immiscible displacements in porous media. Journal of Fluid Mechanics, 189, 165-187. doi:10.1017/S0022112088000953

Lenormand, R., Touboul, E., Zarcone, C. (1988): Numerical models and experiments on immiscible displacements in porous media. J. Fluid Mech. 189, 165–187 in porous media. J. Fluid Mech. 189, 165–187

Landry, C.J., Karpyn, Z.T., Ayala, O. (2014). Transp Porous Med 103: 449. https://doi.org/10.1007/s11242-014-0311-x

Li Chen, Qinjun Kang, Bruce A. Robinson, Ya-Ling He, and Wen-Quan Tao (2013). Phys. Rev. E 87, 043306

Liu, H., Valocchi, A.J., Kang, Q. et al. (2013). Transp Porous Med 99: 555. https://doi.org/10.1007/s11242-013-0200-8

McCloud, K.V., Maher, J.V. (1995). Experimental perturbations to Saffman-Taylor flow. Phys. Rep. 260, 139– 185

Manickam, O., Homsy, G.M. (1995). Fingering instabilities in vertical miscible displacement flows in porous media. J. Fluid Mech. 288, 75–102

M. Latva-Kokko, D.H. Rothman. (2005). Phys. Rev. E 72, 046701

Mukherjee, Partha P. (2010). "Pore-Scale Modeling of Two-Phase Transport in Polymer Electrolyte Fuel Cells - Progress and Perspective". United States.

Nakken. (2012). Fluid Displacements during Multiphase Flow Visualized at the Pore Scale using Micromodels, Master Thesis University of Bergen.

P. G. Saffman., G. I. Taylor. (1958). The penetration of a fluid into a porous medium or Hele-Shaw cell containing a more visous fluid. Proc. Royal Society, 245, 312-329.

Park, C.W., Homsy, G.M. (1985). The instability of long fingers in Hele-Shaw flows. Phys. Fluids 28, 1583– 1585

Peaceman, D.W., Rachford, H. Jr. (1962). Numerical calculation multidimensional miscible displacement. Soc. Pet. Eng. J. 2, 327–339

Piri, M., Blunt, M.J. (2005). Three-dimensional mixed-wet random pore-scale network modeling of two- and three- phase flow in porous media, I. Model description. Phy. Rev. E71, 026301

Psihogios, J., Kainourgiakis, M.E., Yiotis, A.G. et al. (2007). Transp Porous Med.70: 279. https://doi.org/10.1007/s11242-007-9099-2

Regaieg, Mohamed; McDougall, Steven Robert; Bondino, Igor; Hamon, Gerald. (2017). Finger Thickening during Extra-Heavy Oil Waterflooding: Simulation and Interpretation Using Pore-Scale Modelling.

Ramstad, T., Idowu, N., Nardi, C. et al. (2012). Transp Porous Med 94: 487

R. S. Maier, D. M. Kroll, Y. E. Kutsovsky, H. T. Davis, and R. S. Bernard. (1998). Phys. Fluids 10 1

Singh, B., Azaiez, J. (2001). Numerical simulation of viscous fingering of shear-thinning fluids. Can. J. Chem. Engg. 79, 961–967

Succi, S. (2001). The lattice Boltzmann equation for fluid dynamics and beyond. Oxford.

Schulz, V.P., Wargo, E.A., Kumbur, E.C. (2015). Transp Porous Med.107: 13.

Vogel, H. J. and Roth, K. (1998). A new approach for determining effective soil hydraulic functions. European Journal of Soil Science, 49: 547–556. doi:10.1046/j.1365-2389.1998.4940547.x

Youngseuk Keehm, Tapan Mukerji., Amos Nur. (2010). 5th Conference and Exposition on Petroleum Geophysics, Hyderabad-2004, India PP 696-703, Relative Permeability Simulation using the Two-phase Lattice-Boltzmann Method

Yortsos, Y.C., Zeybek, M. (1988). Dispersion driven instability in miscible displacement in porous media. Phys. Fluids 31, 3511–3518

VITA

Zhipeng Zhu was born in 1993 in Xi'an, China. He attended China University of Geosciences Beijing and University of Missouri Science & Technology and received bachelor's degree in petroleum engineering in 2013. He is currently pursuing his master's degree in Petroleum Engineering in Louisiana State University, Baton Rouge.